Norwegian University
of Life Sciences

Master's Thesis 2024 30 ECTS
Faculty of Science and Technology

Pressure vessel protection through non-contact acoustic method

Simon Lindahl Jacobsen
Machine, Process, and Product Development

Acknowledgment

This master thesis is dedicated to developing a non-invasive temperature monitoring system for pressure vessels, contributing to safer industrial operations.

First and foremost, I owe a great debt of gratitude to my advisor, Shailendra Singh, for their expert guidance and constant support throughout this research. Their insights were invaluable, especially during moments of uncertainty with my simulations. Their encouragement and support were crucial during these times, and for that, I am deeply thankful.

Additionally, I must acknowledge my fellow students who provided moral support throughout this process. Shared moments of discovery and frustration enriched this experience immensely. Their perspectives and companionship have made this challenging academic endeavor a rewarding and enjoyable experience.

Lastly, I am profoundly thankful to my family and friends for their endless love and encouragement. Their support has been my backbone, helping me to persevere through the demanding moments of this academic journey.

Ås, 15.05.2024

Simon Lindahl Jacobsen

Abstract

This study aims to develop a novel pressure vessel detection system through an acoustic method. This monitoring system is designed to detect temperature changes within the vessel to enable preventative actions and avoid potential equipment failure. The method is based on the principle that the speed of sound is temperature-dependent. The proposed method uses transducers to transmit ultrasonic waves through the vessel. By measuring the time-of-flight of the signal and predetermining the material and geometry of the vessel, it is possible to calculate the temperature of the encapsulated gas. A time-of-flight range is established based on the operating temperature of the vessel. If the time-of-flight of a transmitted signal is detected outside of the established range, it indicates a temperature change.

This study used a non-invasive ultrasonic method to address the challenge of detecting temperature changes inside a pressure vessel. Through a series of simulations, the computational model demonstrated its capability to measure the time-of-flight of ultrasonic waves accurately. Key findings from the test cases provided the following insights:

- Test Case 1 confirmed the model's validity compared to previous work.
- Test Case 2 demonstrated improvements in the geometric model, reducing the time-of-flight and showing stronger pressure signals at the receiver.
- Test Case 3 revealed that material changes to steel did not significantly affect the time-of-flight due to the minimal thickness of the plates, but significantly weakened the signal strength.
- Test Case 4 highlighted the model's sensitivity to extreme temperatures, where the increased temperature substantially shortened the time-of-flight and weakened the signal strength.

The conclusion of this study states that a computational model has established the method's feasibility; however, work is required to develop a functional prototype. The proposed further work involves conducting physical experiments to translate these computational findings into practical applications and validate the model under real-world conditions.

Contents

List of figures

List of tables

1 Introduction

Temperature and pressure monitoring is a crucial part of industrial instrumentation, applicable in pressure vessels. A pressure increase within a pressure vessel can potentially have catastrophic consequences for both personnel and equipment [1]. Therefore, it is crucial to implement a system that can accurately and reliably detect these changes to enable preventative actions. Pressure vessel failure can be predicted by monitoring the changes in the pressure before a catastrophic failure is reached. Since pressure and temperature are linearly dependent in a closed volume, monitoring temperature provides the pressure inside the vessel [2]. Standard methods of temperature monitoring, such as thermocouples, are accurate and reliable but invasive [3, 4]. These methods require direct contact with the encapsulated gas, causing concerns about regular calibration, leakage, and cost [3]. Developing an accurate and reliable non-invasive method of detecting temperature change would enhance safety and cost efficiency.

This study introduces a non-invasive acoustic temperature change detection system for pressure vessels. The method is based on the principle that the speed of sound is temperature-dependent. By measuring the time-of-flight and predetermining geometry and wall material, it is possible to predict the temperature of the encapsulated gas. However, this method will not be used as a precise temperature predictor but rather as a detection system for rapid temperature changes. This will be achieved by establishing an allowed time-of-flight range determined by the operating temperature.

1.1 Problem Statement:

Despite the necessity for accurate and reliable temperature monitoring in pressure vessels to prevent equipment failure and ensure personnel safety, current methods predominantly rely on invasive techniques [1, 4]. These methods pose challenges regarding cost and increased leakage risks. Therefore, there is a need to develop a non-invasive temperature detection system that can offer comparable accuracy and reliability without the drawbacks associated with invasive approaches.

1.2 Primary objectives:

The primary objective of this thesis is the following:

1. Detect the temperature and corresponding pressure increase inside a closed containment, through non-invasive acoustic measurement method, so that preventive actions can be taken before equipment failure.
2. In the first step, FEM simulation will be performed to validate the idea.
3. In the second step, a prototype container will be used to measure the effects of pressure wave propagation in different boundary conditions.

1.3 Limitations:

The limitation of this thesis is the following:

- The developed models are simplified with gasses considered ideal.
- The geometrical model's dimensions are simplified and do not replicate dimensions of specific pressure vessels, in order to minimize computational complexity.
- Only air will be investigated as encapsulated gas.
- The computational model was only available for two weeks due to license restrictions, resulting in limited time for model refinement.

1.4 Structure of the thesis:

The thesis will include a literature review, theoretical framework, application, analytical calculations, computational model, and simulations. This structure will give the reader a comprehensive understanding of the topic and validate the work from theory to computational model.

It begins with a literature review in Chapter 2. This chapter examines previous work on temperature monitoring in pressure vessels, setting the context for the rest of the thesis. Chapter 3 covers the theoretical framework, providing insight into the physics of wave propagation, which is fundamental for developing the simulation model. Chapter 4 describes the application of a non-invasive temperature detection system in a specific pressure vessel, namely medium voltage switchgear. Chapter 5 details the geometrical parameters of a prototype and conducts analytical calculations for the time-of-flight of a transmitted signal. These calculations will be used to validate the simulation model. The setup of the simulation model is outlined in Chapter 6, including parameters, geometry, materials, boundary conditions, and mesh configurations. Chapter 7 conducts four simulations, starting with a validation model and progressively testing different variables and their effect on wave propagation. Chapter 8 discusses the result, comparing the test cases to analyze the effects of the variables introduced in the simulations. Chapter 9 concludes the study, reflecting on the findings and suggesting areas for further work, focusing on the next step toward developing a functional prototype.

This structure ensures a thorough investigation of the topic. It starts with a review of existing literature, moves through theoretical exploration, practical applications, and simulations, and concludes with a discussion of the outcomes and proposals for further work.

1.5 Artificial intelligence statement

Artificial intelligence has been used in this thesis in accordance with the guidelines given by Norges Miljø- og biovitenskapelige universitet [5].

It has been used as a tool for improving language and structure and to correct grammatical errors. Additionally, it has served as a search tool for finding specific research papers, utilizing prompts such as “find me a research paper on arc faults.”

2 Literature review

2.1 Pressure vessels

The study [6] investigates the structural effects of mild steel pressure vessels under elevated temperature conditions. This research is significant to scenarios where pressure vessels are exposed to extreme temperature increases, such as fires resulting from accidents or external impacts. The study employs analytical and numerical approaches to explore how high temperatures affect vessel integrity. Key findings reveal that the failure pressure of a vessel decreases approximately linearly with increasing temperature. As the temperature of the vessel increases, its ability to withstand internal pressure decreases linearly. Furthermore, the study reveals that the temperature gradient from the outer to the inner wall of the tank does not significantly impact the pressure required for tank failure. Indicating that the failure of the vessel is affected by the overall elevated temperature rather than the gradient across the wall.

Furthermore, [1] examines six significant pressure vessel failures, focusing on the consequences of such incidents. These failures demonstrate a wide range of potential consequences, including safety hazards, economic losses, and environmental damages. A notable example is the 1984 Union Oil Co. refinery explosion, which resulted in 17 fatalities and damages exceeding $100 million. The failure was caused by a crack in the vessel, leading to an explosion. This incident underscores the importance of reliable monitoring and rigorous maintenance of pressure vessels to prevent failures.

These studies underscore the risks associated with pressure vessels, particularly under conditions that challenge their structural integrity, such as increased temperatures. The severity of the potential consequences emphasizes the necessity for a reliable monitoring system. Such systems should assess the condition of pressure vessels without contributing to the likelihood of failure.

2.2 Switchgear

A detailed analysis of the electrical arc phenomenon is provided in [7], with a particular focus on thermionic emission. An electrical arc is characterized by the continuous electrical discharge between two electrodes through a gas, such as air, when a sufficient voltage is applied. The study highlights thermionic emission as critical for a sustaining arc. The phenomenon where electrons are released from the cathode due to heat, traveling to the anode and maintaining current flow. The thermal emission is most intense at the cathode, where temperatures are highest. Although precise temperature measurements within an arc are challenging, the study reports temperatures exceeding 3000° K.

A common type of pressure vessel is described in [7]: medium-voltage air-insulated switchgear (AIS). The study explores the effect of internal arc faults occurring in AIS, focusing on the resulting pressure rises within these vessels. Hot gases are released during arc faults, causing significant pressure

increases that pose risks to the structural integrity of switchgear rooms. The study emphasizes the importance of robust room design with pressure relief ducts to minimize damage if an arc fault occurs.

The study [8] introduces a novel approach for simulating arc movement and burnthrough predictions based on first principles, avoiding the necessity for empirical data. Traditional methods for estimating the effects of internal arcs in switchgear rely heavily on empirical data, which does not account for the arcs' dynamic and leads to unreliability in their pressure rise predictions. This simulation model allows for precise prediction of arc movements, voltage fluctuations, and resulting thermal and pressure stresses that can lead to catastrophic failures.

Switchgears are pressure vessels vulnerable to internal pressure increases from arc faults, which can produce extreme temperatures and pressures. The mentioned studies demonstrate the challenges in predicting these events and their potential to cause structural damage. Reliable monitoring systems are crucial for detecting early signs of temperature and pressure changes, allowing for preventative measures.

2.3 Non-invasive temperature monitoring

A novel sonic sensor method for measuring gas pressure within a commercial pressure vessel is discussed in [9]. This method employs a sonic transducer to induce oscillating forces on the vessel's surface, sweeping through frequencies to excite resonant vibrations in the gas [9, 10]. The amplitude of these vibrations is captured and utilized to determine the resonant frequency of the gas, which varies with the gas’s pressure, temperature, and geometry of the vessel. By predetermining the latter three, measuring the pressure of the encapsulated gas is possible.

The study [11] introduces a non-contact ultrasonic method for gas flow metering using air-coupled leaky Lamb waves. It is only meant to show proof of principle experimentally. Therefore, a simplified model of a gas flow duct was investigated. The model consists of two isotropic plates with gas flowing between them. Transducers are used to excite Lamb waves in the plates, causing Leaky Lamb waves to travel through the duct. The gas flow within the duct shifts the wave field. Two transmissions are done in opposite directions. The flow is determined by comparing the wave shift from the two transmissions.

The feasibility of using acoustic methods utilizing transducers to measure properties of encapsulated gas in pressure vessels and as flow metering in pipes has been documented in [9] and [11]. These non-invasive techniques offer a promising possibility for monitoring the temperature of an encapsulated gas without the need for direct contact, thereby reducing the risks associated with traditional methods. The study [11] proves the feasibility of transmitting and detecting ultrasonic waves through a duct, similar in geometry to a simplified pressure vessel. The model described in [11], initially applied as a flow meter, will be used to validate the simulations and expand on to test the wave propagation effect of different variables, such as material, temperatures, and geometries.

3 Theoretical framework

3.1 Sound waves

All sound waves are different types of mechanical waves propagating through a medium. The mechanical wave transmits energy through a medium by the vibrations of the particles of the medium [12]. When a material remains within its elastic threshold, the particles oscillate elastically about their equilibrium position. A particle displaced from its equilibrium position will experience internal restoring forces. These restoring forces, combined with the inertia of the individual particles, are the cause of the oscillatory motion of a medium. Based on the movement of the particles in a medium, mechanical waves are categorized into two fundamental types: longitudinal waves and transverse waves [13].

3.1.1 Longitudinal waves

The particle displacement in a longitudinal wave is parallel to the direction of wave propagation, as illustrated in Figure 1. However, the particles do not move along with the wave. They oscillate backward and forward about their individual equilibrium position. This oscillation creates high-pressure and low-pressure areas, subsequently called compression and rarefaction. This phenomenon causes a density fluctuation to propagate through the medium, which is the process that defines the wave [14].

3.1.2 Transverse wave

The particle displacement in a transverse wave is perpendicular to the direction of wave propagation, as seen in Figure 2. If the transverse wave propagates from left to right, the particles oscillate up and down about their equilibrium position [14]. Transverse waves are relatively weaker than longitudinal waves and can only propagate effectively through acoustically solid materials. Hence, gases and liquids are mediums not suited for transverse waves. However, it is common for waves to be a combination of longitudinal waves and transverse waves, forming different wave modes[13].

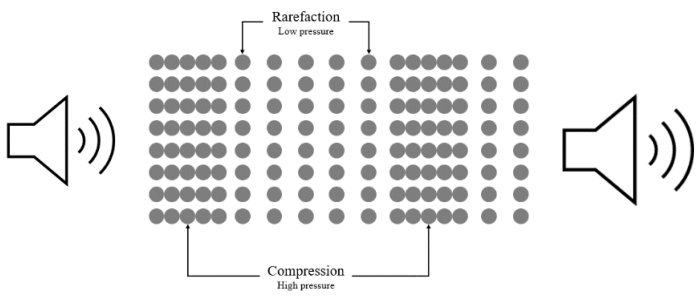

Figure 1: Dynamics of longitudinal waves.

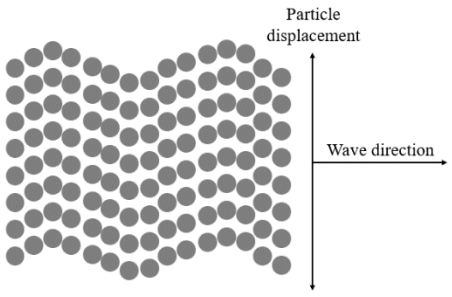

Figure 2: Dynamics of transverse waves.

3.2 Wave propagation in elastic materials

As described earlier, the propagation of a sound wave results from the elastic oscillation of individual particles within a medium. An ultrasonic wave can be considered an infinite number of oscillating masses connected by massless elastic springs in a uniform pattern, as illustrated in Figure 3. The individual particles are affected by their adjacent particles [13]. A mass on a spring has a single resonant frequency, which is determined by its spring constant and mass. The spring constant represents the restoring force exerted by the spring per unit length of displacement [13]. As described by Hook's law, the displacement of a particle is directly proportional to the force attempting to restore the particle to its equilibrium position:

$$f = -kx \tag{3.1}$$

Newton's second law states that an applied force on a particle equals its mass times its acceleration. Hook's law states that the restoring force in a spring is proportional to the displacement and acts in the opposite direction to the applied force. Combining these in equations (3.2) shows that acceleration is directly proportional to displacement, as mass and spring constant are constant. Therefore, the time it takes for a particle to return to its equilibrium position is independent of the force applied. Hence, the speed of sound is constant for a given material regardless of the applied force, assuming material conditions remain constant [13].

$$ma = -kx \tag{3.2}$$

Where:

- f = restoring force [N].
- k = spring constant [N/m].
- x = displacement [m].
- m = mass [kg]
- a = acceleration [m/s^2]

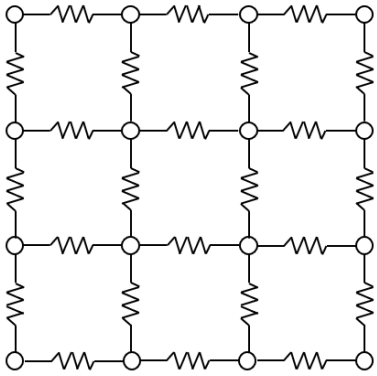

Figure 3: Elastic spring system.

3.3 Speed of sound

The speed of sound varies with respect to the medium through which it propagates. Materials with different atomic mass and spring constant have consequently different speeds of sound. The density of a material is directly related to atomic mass, and the spring constant is considered the material's elastic property. The general expression for the speed of a mechanical wave is [13, 15]:

$$v = \sqrt{\frac{elastic\ property}{inertial\ property}} \tag{3.3}$$

Additionally, satisfying the wave equation [15, 16]:

$$\frac{\partial^2 y(x,t)}{\partial x^2} = \frac{1}{v^2}\frac{\partial^2 y(x,t)}{\partial t^2} \tag{3.4}$$

3.3.1 Speed of sound in solids

Solid supports longitudinal and transverse waves. For longitudinal waves, the speed of sound depends on the material's elastic property, Young's Modulus, and its inertial property, density. The speed of a longitudinal wave is expressed as [15, 17]:

$$c = \sqrt{\frac{E}{\rho}} \tag{3.5}$$

The speed of sound for transverse depends on the materials elastic property, shear modulus and its inertial, property density, expressed as [13]:

$$c = \sqrt{\frac{G}{\rho}} \tag{3.6}$$

Where:

- c: speed of sound [m/s].
- E: Young's Modulus [N/m^2].
- G: shear modulus [N/m^2].
- ρ: density [kg/m^3].

3.3.2 Speed of sound in air

As stated earlier, gasses only support longitudinal waves under normal conditions. The speed of sound in air is calculated using the adiabatic compressibility, which is linked to the adiabatic index [15, 18]. If the air is considered ideal, the elastic property, the bulk modulus, is expressed as [15, 19]:

$$K = \gamma * p \tag{3.7}$$

From the ideal gas law, the pressure is expressed as [15, 19]:

$$p = \frac{nRT}{V} \tag{3.8}$$

And the density is expressed as [15, 19]:

$$\rho = \frac{nM}{V} \tag{3.9}$$

By substituting the elastic property with the bulk modulus, equation (3.7) in the general speed of wave equation (3.3), the speed of sound in an ideal gas is expressed as [15, 19]:

$$c = \sqrt{\frac{K}{\rho}} = \sqrt{\gamma \frac{p}{\rho}} = \sqrt{\gamma \frac{\frac{nRT}{V}}{\frac{nM}{V}}} = \sqrt{\gamma \frac{RT}{M}} \tag{3.10}$$

Where:

- c: speed of sound [m/s].
- K: bulk modulus [Pa].
- ρ: density [kg/m^3].
- γ: adiabatic constant.
- p: pressure [Pa].
- n: number of moles.
- R: gas constant [J/(mol*K)].
- T: temperature [K].
- V: volume [m^3].
- M: molar mass [kg/mol].

3.3.3 Temperature affecting the speed of sound

From the speed of sound equations (3.5), (3.6,) and (3.10), it is clear temperature of a medium affects the speed of sound. Heat is a form of kinetic energy. Particles in a medium with elevated temperatures have more energy, causing the particles to vibrate faster. This velocity increase causes soundwaves to propagate through the medium at a higher rate [13].

3.4 Transmission and reflection

3.4.1 Transmission through an interface

When a sound wave propagating through a medium hits an interface of a second medium, the initial wave splits into two: a reflection and a transmission wave. However, if the initial wave propagates normally to the interface, the equation for fluid mediums can be used, with the only modification being that the speed of sound in the solid is the bulk speed of sound. Both the intensities and the pressure amplitude are affected by this phenomenon. The ratio of these values for the reflected and transmitted wave is determined by the characteristics of the acoustic impedance, the speed of sound in the two mediums, and the angle of the initial wave relative to the interface. However, for a wave traveling normally to the planar interface, only the acoustic impedance should be considered, expressed as [16, 20]:

$$Z = p * c \tag{3.11}$$

Where:

- Z: acoustic impedance [Pa*s/m^3].
- p: equilibrium density of medium [kg/m^3]
- c: speed of sound in medium [m/s].

3.4.2 Transmission through a fluid layer

When a sound wave travels normally through a planar fluid layer, two interfaces must be considered. At each interface, some of the wave energy will transmit through, and some will reflect. The initial wave hits interface 1 at x=0, where the transmitted wave travels into fluid 2, and the reflected wave travels into fluid 1. The ratio of transmission and reflection is dependent on the acoustic impedance *Z* of the fluids. The transmitted wave will travel through the fluid layer before encountering the interface between fluids 2 and 3. Again, at this interface, some wave energy is reflected into fluid 2, and some is transmitted into fluid 3. This reflected wave is "trapped" inside fluid 2, where it will travel back and forth between the interfaces, gradually losing energy. In Figure 4, an initial wave propagating through a fluid layer is depicted, where interface 1 is at x=0, the fluid layer has a length of *L*, *r* denotes the acoustic impedance of the respective fluid, and *P* represents the pressure amplitude of the respective wave [16]. It is important to note that in this study, the acoustic impedance is denoted as Z. The reduction of wave energy of the initial wave as it hits an interface only affects the amplitude. Both the reflected and transmitted waves will have a reduced amplitude compared to the initial wave. The amplitude of the generated wave at the interface is determined by the transmission coefficient and reflection coefficient, expressed as:

$$T = \frac{2 * Z_2}{Z_1 + Z_2} \tag{3.12}$$

Where:

- T: transmission coefficient.
- Z_2: acoustic impedance of medium 2 [Pa*s/m^3].
- Z_1: acoustic impedance of medium 1 [Pa*s/m^3].

$$R = \frac{Z_2 - Z_1}{Z_2 + Z_1} \tag{3.13}$$

Where:

- R: reflection coefficient.
- Z_2: acoustic impedance of medium 2 [Pa*s/m^3].
- Z_1: acoustic impedance of medium 1 [Pa*s/m^3].

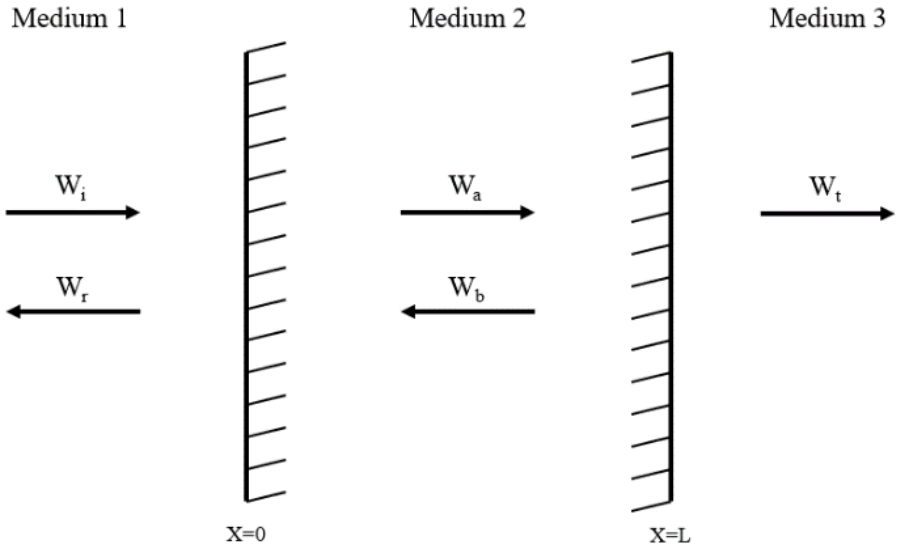

Figure 4: Transmissions and reflection of an initial wave traveling through a fluid layer.

4 Applications

4.1 Internal arc fault in medium voltage switchgear

4.1.1 Medium voltage switchgear

Different types of switchgears are used throughout the electrical grid, categorized into high-, medium- and low- voltage switchgear. In general, a switchgear is a system of integrated circuit protection devices that protect, control and isolate electrical devices. The most critical function is to interrupt the power supply in the event of a power surge, thereby protecting the electrical devices [21, 22].

4.1.2 Arc fault

The primary risk associated with AIS is the possibility of internal arc faults, which is a major personnel safety concern [23]. If an arc is developed in switchgear, it can lead to equipment failure within a few hundred milliseconds [24]. The process of an arc fault in a switchgear can be described as:

1. Compression phase (0-15 ms): The initial phase comprises of a rapid rise in temperature and the formation of a pressure wave. During this phase the system experience maximum pressure.
2. Expansion phase (15-30 ms): Following the compression phase the air and gas starts to move due to pressure difference between arc and surrounding pressure. Commonly, this is when pressure relief ducts are opened. During this phase the pressure declines.
3. Emission phase (30- few 100 ms): Sustained electrical input at the arcing point causes a continuous flow of air and gas. This phase is characterized. With high speed, high temperature, glowing gas flow.
4. Thermal phase: During this phase most of the air has left the cabinet, remaining air heats up to nearly arc temperature. At this time there is high risk for burnthrough [25]. This phase continues until the arc has been cleared.

Although arc faults rarely occur in switchgear, especially causing personal harm, they cannot be disregarded [26]. It is expected that an arc fault occurs in one in every 10,000 switchgears a year [24]. An arc fault is generally caused by material faults, functional faults, incorrect dimensioning, foreign objects, or incorrect cable connections [24, 27]. The main concern with an arc fault in a switchgear is the potential harm to personnel, equipment, and infrastructure. This risk is associated with the high temperatures and pressure waves generated by such a fault. Medium voltage switchgear is often installed in buildings. These building structures must be dimensioned to withstand a potential pressure wave caused by an arc fault in the switchgear [24, 28].

4.1.3 Current solutions

Protection against arc faults is categorized into two systems: passive and active system. The passive system is a preventive measure and is mainly used in low-voltage switchgear. The active system, commonly used in medium voltage switchgear, detects and stops an occurring arc fault. This system is time-sensitive and relies on a rapid response to mitigate damage [24]. The active system must fulfill two criteria:

- Flash from the arc must be detected.
- Rapid current increase must be detected.

If these two criteria are fulfilled a detection will be recognized, and tripping will be initiated by an internal arc fault device (IACD). The arc quenching device (AQD) will be tripped, causing a low resistance path for the current to flow, upstream of the arc fault location. This will drain the arc of energy and effectively extinguish it [24, 29].

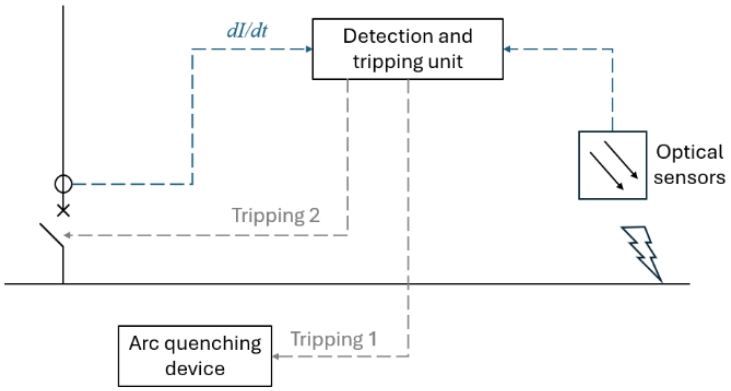

Figure 5: General principle of an active arc fault protection.

4.1.4 Arc fault detection through non-invasive acoustic method

The above-mentioned arc fault protection system is invasive, as it would involve the placement of a light sensor inside the pressure vessel. The non-invasive method described in this thesis will transmit ultrasonic waves through the vessel from the outside, measuring the time-of-flight of the signal. A time-of-flight range will be established based on the vessel's operating temperature. The system will transmit waves continuously with the expected time-of-flight to be within the established range. A signal outside this range is an indication of state change within the vessel.

5 Analytical analysis

In this chapter, an analytical analysis will be conducted. Two simplified geometrical models are developed, simulating a pressure vessel with transducers on the outside. The geometrical parameters will be used to conduct analytical calculations on the time-of-flight of a wave propagating through a vessel in accordance with the method described in Chapter 4.1.4. Further, the results from these calculations will be used to validate the simulation model used in Chapter 7

5.1 Geometric parameters

Two simplified illustrations outlining the 2D models that will be used in the analytical calculations are shown in Figure 6 and Figure 7. The models are meant to showcase a generic case of a vessel with encapsulated air and to study the feasibility of measuring the time-of-flight of a propagating wave. Both models consist of the following five domains:

- Domain 1: Ambient air, including the transmitter.
- Domain 2: First plate.
- Domain 3: Encapsulated air.
- Domain 4: Second plate.
- Domain 5: Ambient air, including receiver.

The only difference between the two models is that one has the transducers at an oblique angle to the plane of the plates, while the other has the transducers normal to the plane of the plates. The difference in transducer setup has implications for the way the sound wave propagates through the box. This will be discussed further in Chapter 7.

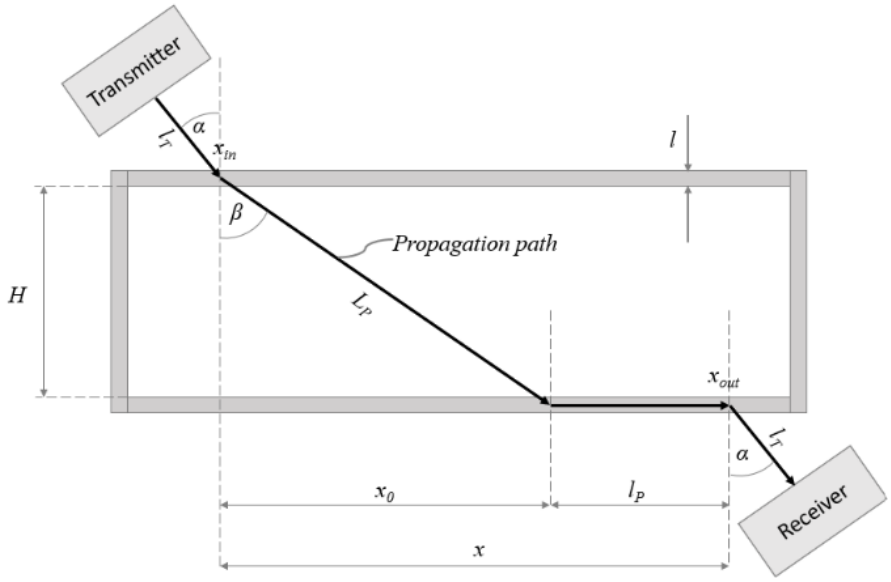

Figure 6: Simple model of angular geometry.

The geometric parameters for the angular case are given in Table 1:

Table 1: Geometric parameters angular case.

Geometric parameters	Symbol	Values [mm]
Plate length	W	370
Plate thickness	l	1
Plate separation	H	90
Transducer height	T_H	20
Transducer width	T_w	40
Length from transducer to plate	l_T	30
Transducer angle	α	50 [°]
Box inlet-outlet propagation length	$x = x_{out} - x_{in}$	150
Leaky Lamb wave angle	β	52.90 [°]
Propagation path length inside the box	L_P	149.110
Horizontal displacement inside the box	x_0	118.885
Horizontal displacement inside plate	$l_P=x - l_p$	31.114

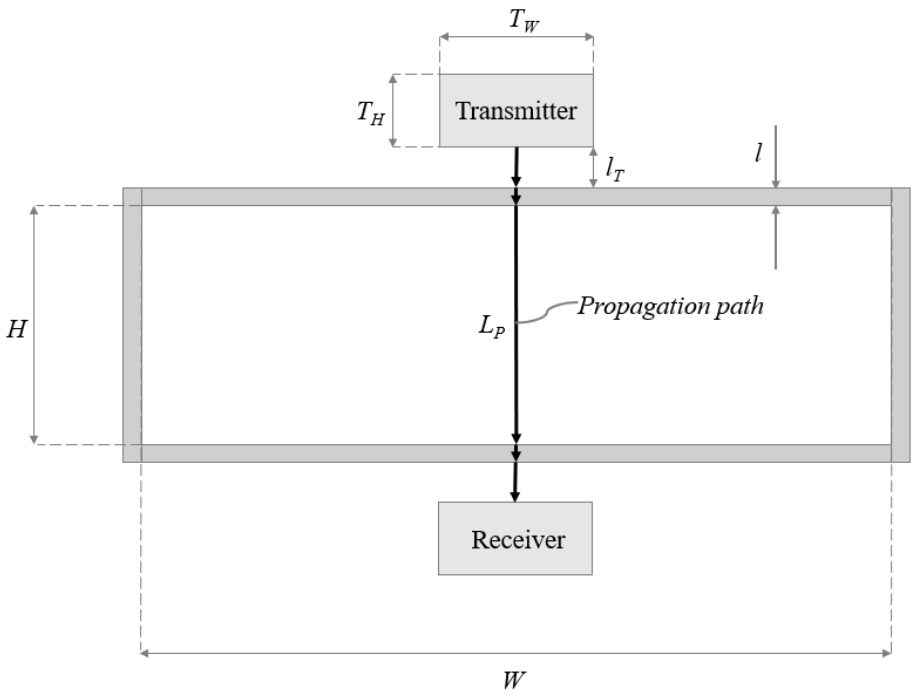

Figure 7: Simple model of normal geometry.

The geometric parameters for the normal case are given in Table 2.

Table 2: Geometrical parameters of normal case.

Geometric parameters	Symbol	Values [mm]
Plate width	W	370
Plate thickness	l	1
Plate separation	L_P=H	90
Transducer height	T_H	20
Transducer width	T_w	40
Length from transducer to plate	l_T	8

5.1.1 Angular case

The propagation path for the angular case can be divided into four parts, as seen in Figure 6. It is important to notice that the length from transmitter and receiver to the plates are the same lengths. The time-of-flight is given by:

$$t_{ToF} = \frac{2 * l_T}{c_{air}} + \frac{L_P}{c_x} + \frac{l_P}{c_{plate}} \tag{5.1}$$

Where:

- t_{ToF}: time-of-flight [s].
- l_T: length from transducer to plate [m].
- L_P: length between plates [m].
- l_P: length inside plate two [m].
- c_{air}: speed of sound in ambient air [m/s].
- c_x: speed of sound in encapsulated air [m/s].
- c_{plate}: speed of sound in plates [m/s].

Since the speed of sound depends on the temperature of the medium (equation (5.2)), any change in the temperature of the enclosed gas in switchgear by an internal arc would lead to a change in time-of-flight (equation (5.1)). So, by continuously monitoring the time-of-flight inside a switchgear, it is possible to predict the occurrence of an internal change in time-of-flight [13]:

$$c = \sqrt{\gamma * R_s * T} \tag{5.2}$$

Where:

- c: speed of sound [m/s].
- γ: adiabatic gas constant for air.
- R_s: specific gas constant for air [J/(kg*K].
- T: temperature [K].

The lengths of the propagation path, given in Table 3, are used together with the speed of sounds, given in Table 5, to calculate the time-of-flight. The calculated time-of-flight, given in Table 4, will be used to validate Test case 1 in Chapter 7.1.

Parameters	Symbol	Value [mm]
Leaky Lamb wave angle	β	52.9 [deg]
Horizontal displacement inside box	x_0	119.0
Transducer to plate	l_T	30.0
Propagation inside box	L_P	149.11
Inside plate two	l_P	118.88

Table 3: Propagation path parameters.

Calculating	Value	Unit
Time-of-flight	6.55E-4	s

Table 4: Analytical calculations value for time-of-flight in angular case.

5.1.2 Normal case

The propagation in the normal case follows a straight vertical path, which reduces the propagation length. The transducers are oriented normally to the plane of the plates, eliminating all angles, and simplifying the calculations. The time-of-flight is expressed as:

$$t_{ToF} = \frac{2 * l_T}{c_{air}} + \frac{2 * l}{c_{plate}} + \frac{L_P}{c_x} \tag{5.3}$$

Where:

- t_{ToF}: time-of-flight [s].
- l_T: length from transducer to plate [m].
- l: length plates [m].
- L_P: length between plates [m].
- c_{air}: speed of sound in ambient air [m/s].
- c_{plate}: speed of sound in plates [m/s].
- c_x: speed of sound in encapsulated air [m/s].

The lengths of the propagation path, given in Table 2, is used together with the speed of sounds, given in Table 5, to calculate the time-of-flight. The calculated time-of-flights, given in Table 6, will be used to validate Test case 2-4 in Chapter 7.2, 7.3, and 7.4.

Material	Density [kg/m^3]	Young's modulus [Pa]	Speed of sound [m/s]
Polycarbonate	1200	2.00E+09	1290
Steel	7850	2.00E+11	5048
Dry air (20 °C)	1.2044	-	343.2
Dry air (4000 °C)	0.083	-	1310

Table 5: Speed of sound in material used in normal cases.

Test case	Speed of sound [m/s]
Test case 2	343.2
Test case 3	343.2
Test case 4	1310.3

Table 6: Analytical calculation values for speed of sound in encapsulated air for normal cases.

Test case	Time-of-flight [s]
Test case 2	3.10E-4
Test case 3	3.09E-4
Test case 4	1.17E-4

Table 7: Analytical calculation values for time-of-flight for normal cases.

6 Computational model

This chapter presents the computational model that was developed to simulate wave propagation under the same conditions as described in Chapter 5. The entire simulation was conducted in COMSOL Multiphysics. The simulation model was developed by the following steps:

- Establish a 2D component.
- Defining global definitions, parameters, and variables.
- Building the geometric model.
- Defining materials and their properties.
- Specify the domains and boundary conditions.
- Create suitable mesh.
- Compute solutions.
- Postprocessing and visualizing results.

6.1 Definitions and parameters

The following parameters are defined in Table 8:

Table 8: Parameters defined in the simulation model.

Name	Expression	Value	Description
c_0	343.2[m/s]	343.2 m/s	Speed of sound in dry air
f_0	100[kHz]	1E5 Hz	Carrier signal frequency
ω_0	2*pi*f0	6.2832E5 Hz	Carrier signal angular frequency
T_0	1/f0	1E-5 s	Carrier signal period
A	0.1[mm/s]	1E-4 m/s	Velocity signal amplitude

These parameters are used to modulate a Gaussian pulse that will be used to apply a velocity to the transmitting diaphragm, as illustrated in Figure 8 and expressed as:

$$v_n(t) = A * e^{-(f_0(t-3T_0)^2)} * \sin(\omega_0 * t) \quad (6.1)$$

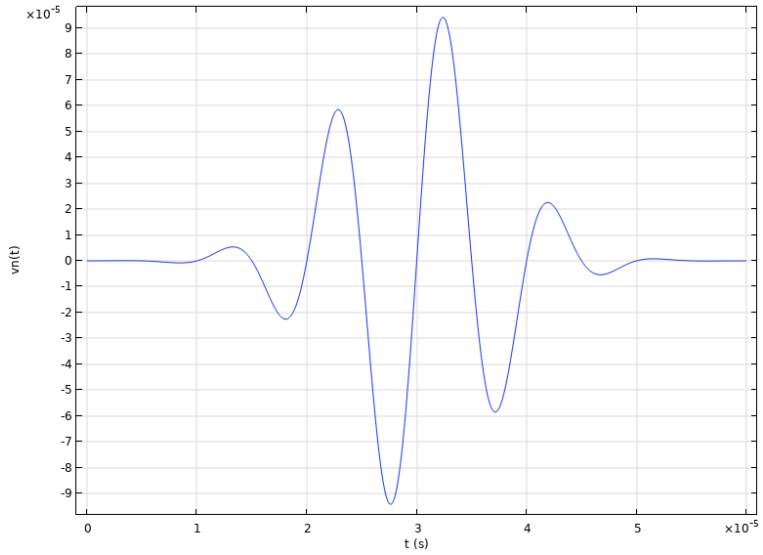

Figure 8: Modulated Gaussian pulse.

6.2 Geometric parameters

The 2D geometric model is based on the simplified models, shown in Figure 9 and Figure 10, consisting of five domains, as described in 5.1. Two geometric models are built, with the only difference being the orientation of the transducer and the distance between the transducer and plate. The model with angled transducers will be used in Test case 1, while the other model will be used in Test case 2-4. The geometric models used in the simulations are seen with parametric values in Figure 9 and Figure 10.

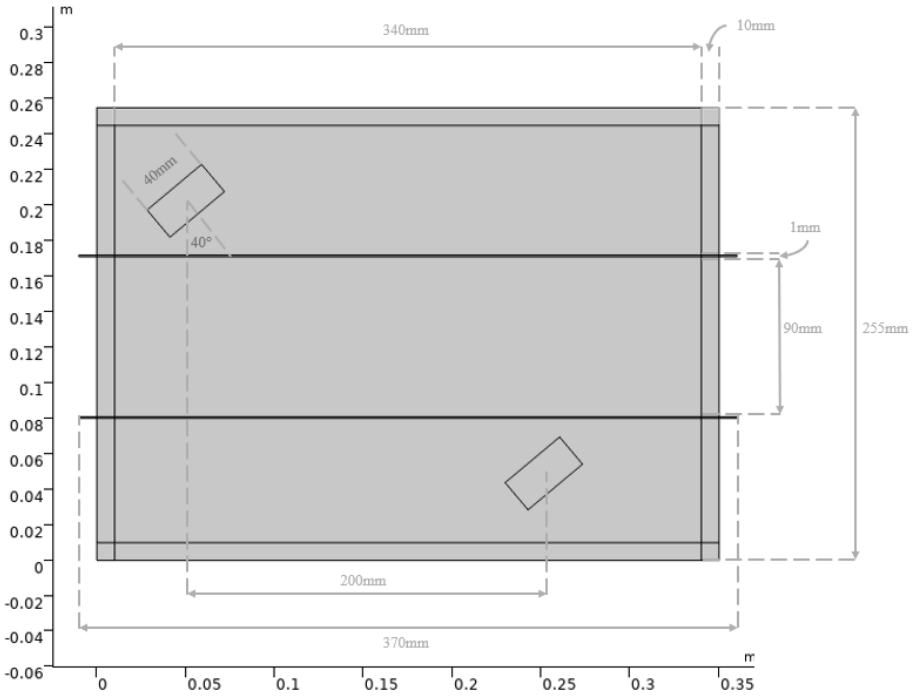

Figure 9: Geometric simulation model used in test case 1.

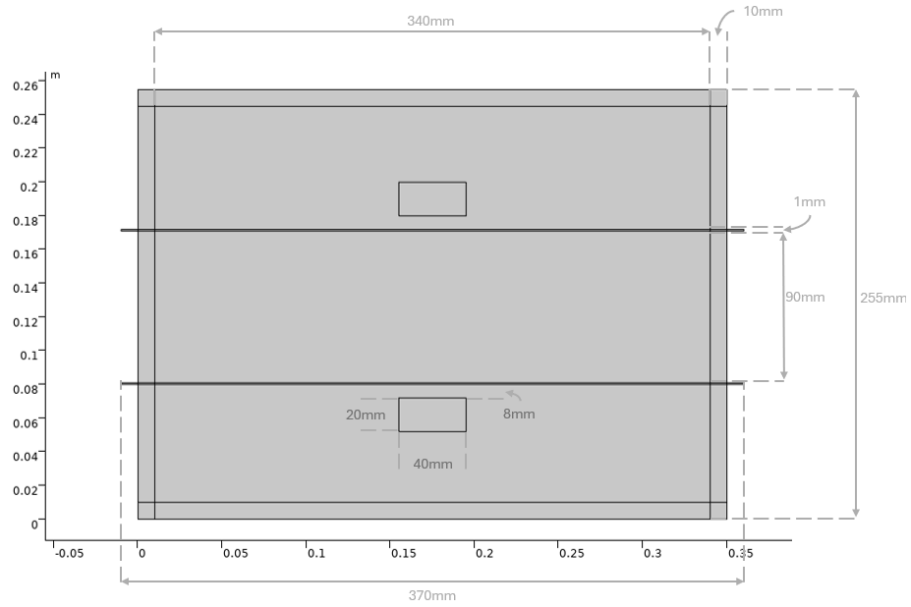

Figure 10: Geometric simulation model used in test case 2-4.

6.3 Material properties

Three different materials were used in the series of simulations conducted. In Test case 1, only ambient air is used as gas and polycarbonate for the plates, which is the same as in [11]. The same materials are used in Test case 2. Since it is of interest to test materials with higher acoustic impedance, steel is used for the plates in Test case 3. Additionally, it is of interest to model the propagation time of sound waves at elevated temperatures; in Test case 4, the speed of sound at 4000 °C was used. The properties of these materials are presented in Table 9.

Table 9: Material properties for materials used in simulations.

Material	Density [kg/m^3]	Young's modulus [Pa]	Speed of sound [m/s]
Air 20 °C	1.2044	-	343.2
Air 4000 °C	0.0826	-	1310.3
Polycarbonate	1200	3.66E09	1290
Steel	7850	2.00E11	4000

6.3.1 Simulation governing equations and numerics

The governing equations describe the transient propagation of linear acoustic waves. These equations consist of first-order transient linearized continuity and momentum equations [30], expressed as:

$$\frac{1}{\rho c^2}\frac{\partial p_t}{\partial \mathrm{t}} + \nabla \cdot u_t = Q_m \tag{6.2}$$

$$\rho \frac{\partial u_t}{\partial \mathrm{t}} + \nabla \cdot (p_t I) = q_d \tag{6.3}$$

Where:

- ρ: fluid density [kg/m^3].
- c: speed of sound [m/s].
- p_t: total acoustic pressure [Pa].
- t: time [s].
- u_t: total acoustic velocity [m/s].
- Q_m: domain source.
- q_d: domain source.

The simulation employs a time-explicit discontinuous Galerkin method to model the transient propagation of linear acoustic waves [31]. This condition utilizes the discontinuous Galerkin finite element method (dG-FEM) to solve the governing equation [32]. This approach resolves acoustic pressure and velocity fields over time and is simulated in COMSOL Multiphysics, ensuring precise spatial and temporal resolution of wave propagation [30].

6.4 Boundary conditions

6.4.1 Non-reflection boundary condition

A non-reflection boundary condition was applied to the outer edges of the environment and the protrusions of the plates in the geometric model. This boundary condition establishes a relationship between the local total acoustic pressure and the normal acoustic velocity defined by the acoustic impedance [30]. This relationship is expressed as:

$$n \cdot u_t(t) = \frac{p_t(t)}{Z_i} \quad [6.4]$$

Where:

- $n \cdot u_t(t)$: normal acoustic velocity as a function of time [m/s].
- $p_t(t)$: total acoustic pressure as a function of time [Pa].
- Z_i: acoustic impedance [Pa*s/m]

In this simulation, the impedance is set to match the characteristic specific impedance of the material, denoted $Z=\rho*c$, effectively causing the boundary to be non-reflective [16, 30].

6.4.2 Internal velocity boundary condition

An internal velocity boundary condition was applied to the transmitter to simulate the vibrating diaphragm in the transducer. This condition ensures that the total normal velocity is consistently defined on both the upward and downward sides of the boundary [30], expressed by the equations:

$$u_{t,up} \cdot n = v_0(t) \cdot n = v_n(t) \tag{6.5}$$

$$u_{t,down} \cdot n = v_0(t) \cdot n = v_n(t) \tag{6.6}$$

Where:

- $u_{t,up} \cdot n$: normal acoustic velocity on the upper side of the boundary [m/s].
- $u_{t,down} \cdot n$: normal acoustic velocity on the lower side of the boundary [m/s].
- $v_0(t) \cdot n$: normal velocity of boundary as a function of time [m/s].
- $v_n(t)$: defined normal velocity function [m/s]

The imposed normal velocity function, defined as a Gaussian pulse as detailed in Chapter 6.1, modulates the dynamics of the boundary.

6.4.3 Internal material transition boundary condition

A material transition boundary condition was applied to the plates in the geometric model to manage variations in material properties across interior boundaries. Implemented using the discontinuous Galerkin method, this boundary condition ensures the continuity of both total pressure and normal acoustic velocity across the transition[30, 32]. The boundary condition is expressed as:

$$p_{t,down} = p_{t,up} \tag{6.7}$$

$$n \cdot u_{t,down} = n \cdot u_{t,up} \tag{6.8}$$

Where:

- $p_{t,down}$: total acoustic pressure on the lower side of the boundary [Pa].
- $p_{t,up}$: total acoustic pressure on the upper side of the boundary [Pa].
- $n \cdot u_{t,down}$: normal acoustic velocity on the lower side of the boundary [m/s].
- $n \cdot u_{t,up}$: normal acoustic velocity on the upper side of the boundary [m/s].

This condition ensures that the physical quantities, such as pressure and velocity, remain continuous, despite the material changes.

6.4.4 Mesh

In the simulation, the mesh configuration includes a maximum element size of 0.004m and a minimum size of 0.001m, with a maximum element growth rate of 2. A curvature factor of 0.3 and a resolution for narrow regions of 0.9. A mapped mesh method was applied to domains 2-4 and the environment's edges, involving four iterations and a maximum element depth of four. For domains 1 and 5, a free quad mesh was used. A detailed mesh of test case 1 can be seen in Figure 11.

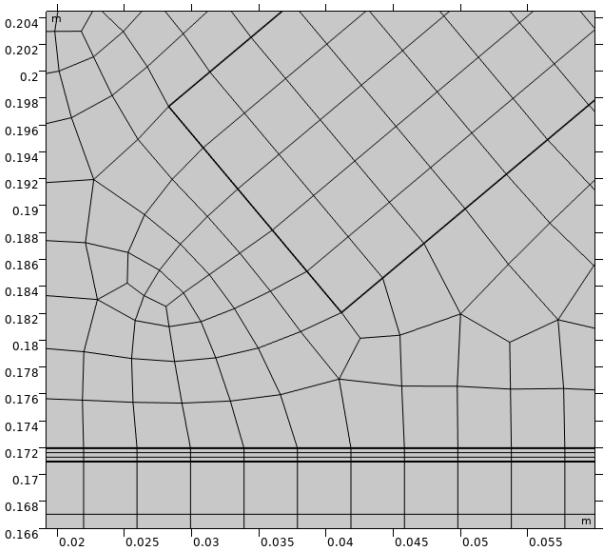

Figure 11: Detailed mesh of test case 1 model.

7 Simulations

Four different acoustic simulations in COMSOL Multiphysics® are conducted using the “pressure acoustic, time explicit” interface. The simulations are divided into Test case 1-4, with variation in geometry, materials, and temperature. The results from each test case are compared to the analytical calculations conducted in Chapter 5. The following simulations are presented in this chapter:

- Test case 1: Angular geometry – polycarbonate material – ambient temperature.
- Test case 2: Normal geometry – polycarbonate material – ambient temperature.
- Test case 3: Normal geometry – steel material – constant temperature.
- Test case 4: Normal geometry – polycarbonate material – high temperature.

There are two different geometries used. In test case 1, the transducers are at an oblique angle in relation to the plane of the plates, as seen in Figure 6. This aligns with the geometric parameter in [11], aiming for validation by expecting a similar time-of-flight. Test cases 2-4 feature transducers positioned normally on the plates. This geometry is shown in Figure 7. The following subchapters describe each simulation setup and result, furthermore discussing its validity and implications.

7.1 Test case 1: Angular – polycarbonate

7.1.1 Setup

Test case 1 is built in as a replica of the model simulated in [11]. It has the same geometry parameters, material, and temperature conditions, as shown in Figure 6 and listed in Table 1, to validate dG-FEM against stabilized FEM method of [11]. The model comprises five domains, as described in Chapter 5. Domain 1 and 5, where the transducers are located, consist of ambient air at 20 °C. Domains 2 and 4 consist of polycarbonate plates. Domain 3 consists of the encapsulated air set to 20 °C.

The following series of figures (Figure 12-Figure 16) depicts the propagation of the ultrasonic sound pulse from transmitter, through each domain, to the receiver. Each figure displays five color scales, showcasing the total acoustic pressure in each domain. Thus, the color scales illustrating the wave propagation are domain-specific (from 1 to 5).

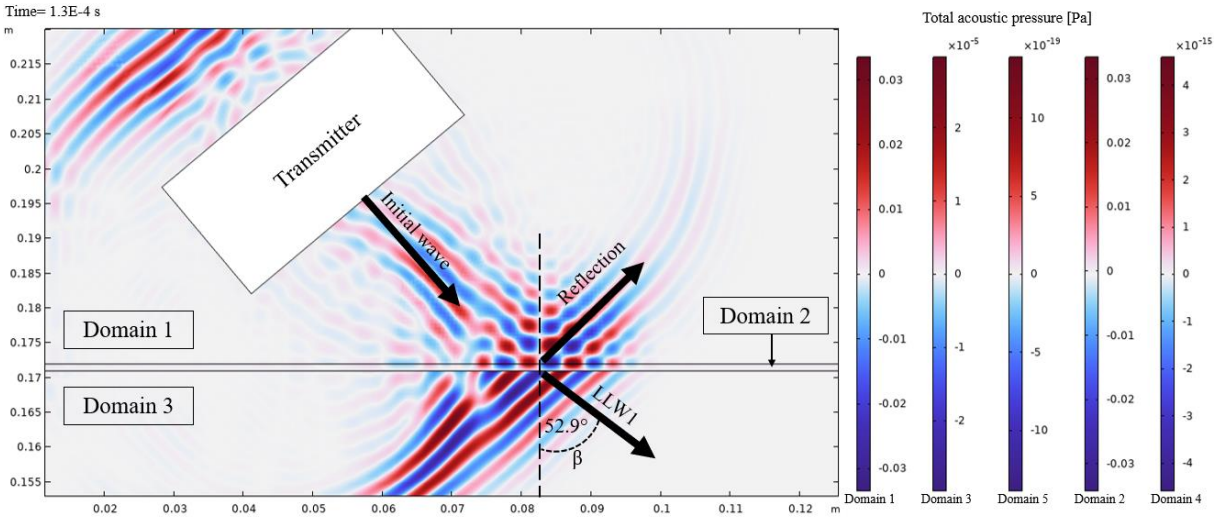

Figure 12: Test case 1 COMSOL simulation zoomed in at 1.3E-4 s.

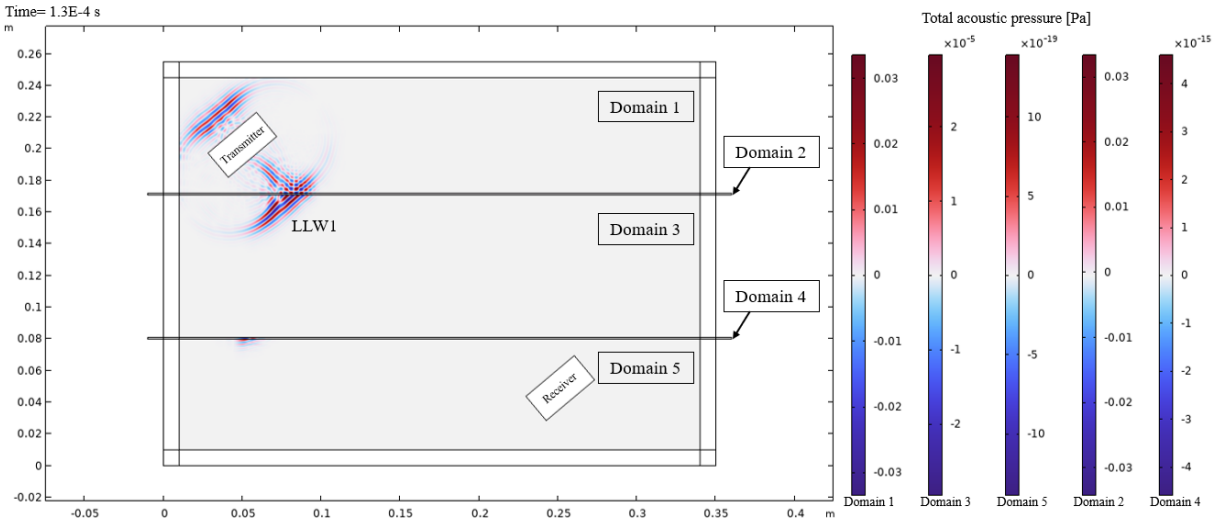

Figure 13: Test case 1 COMSOL simulation at 1.3E-4 s.

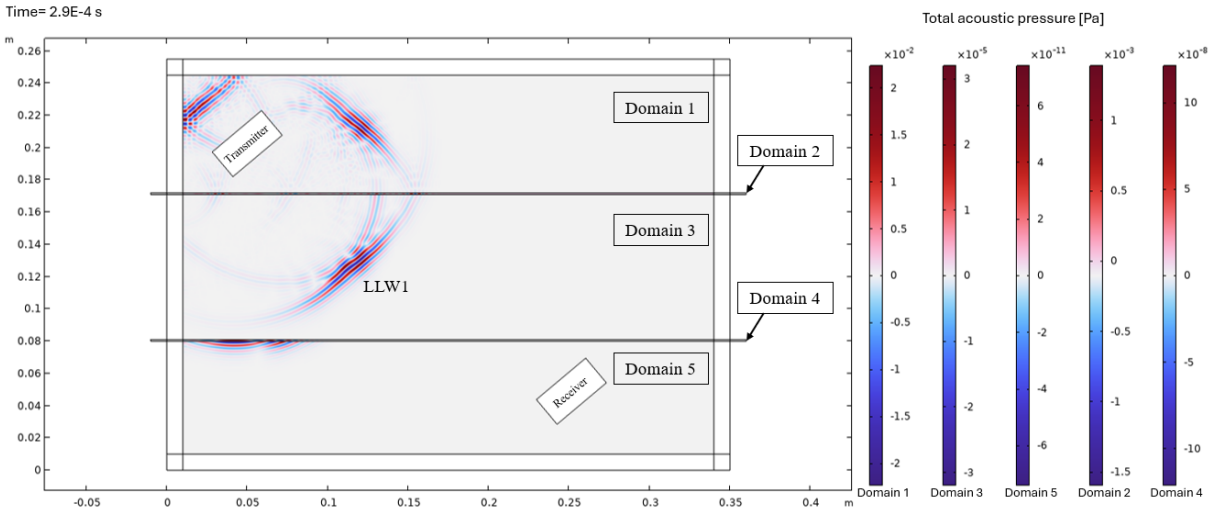

Figure 14: Test case 1 COMSOL simulation at 2.9E-4 s.

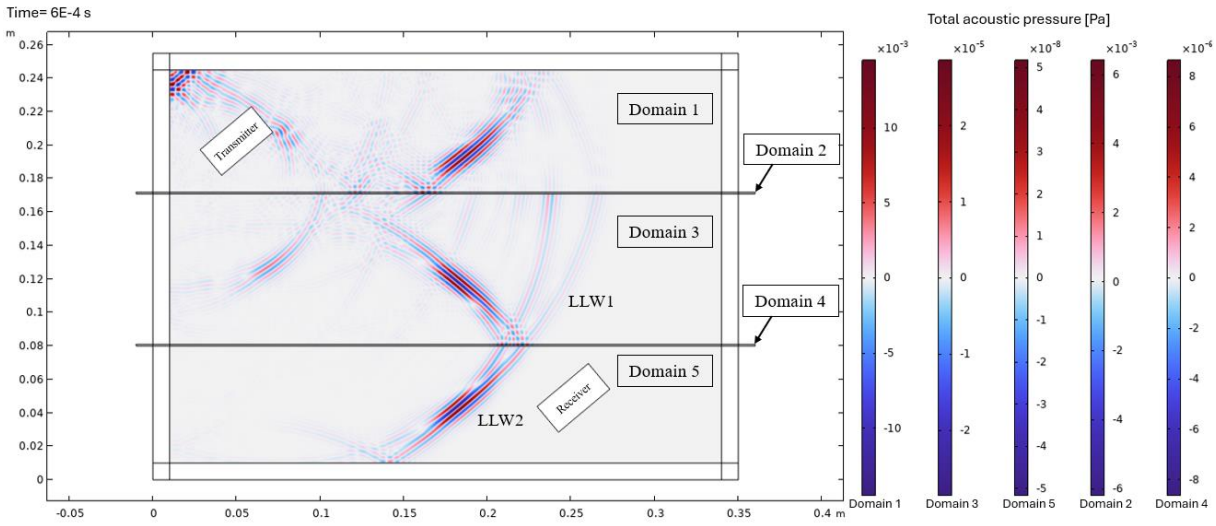

Figure 15: Test case 1 COMSOL simulation at 6.4E-4 s.

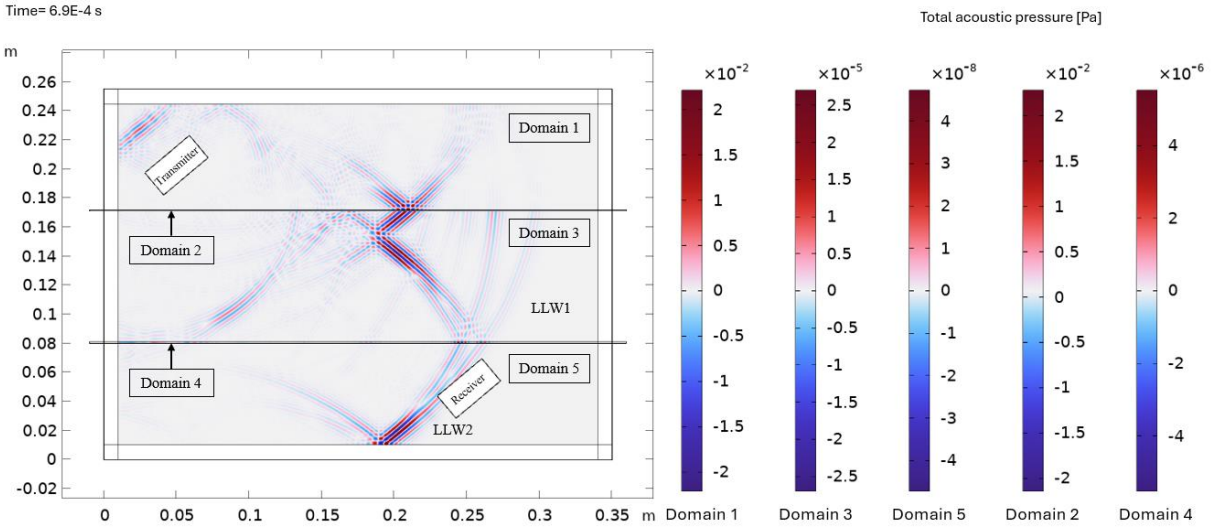

Figure 16: Test case 1 COMSOL simulation at 6.9E-4 s.

7.1.2 Simulation results and analysis

Figure 12 provides a detailed view of the initial propagation path of the ultrasonic sound pulse. The initial wave travels from the transmitter, impacting the interface of domain 2 at 1.30E-4 s. At the interface, the initial wave splits into two. Most of the energy is reflected back into Domain 1; the rest is transmitted into Domain 2. The refraction angle of the transmitted wave is 52.9 °, in accordance with Snell's law. Figure 13 provides an overview of the entire model at the same time step as Figure 12. At this moment, the wave has traveled through domains 1 and 2, continuing into domain 3. Figure 14 captures the wave as it propagates through the encapsulated air in domain 3. In this test case, the temperature of the encapsulated air in domain 3 is set to 20 °C. Hence, the wave propagates through domain 3 at a speed of 343.2 m/s defined as material property of the domain. By the time 6.40E-4 s, in Figure 15, the wave has reached domain 4, where most of the wave is reflected and the rest is refracted. The wave impacts the receiver at 6.90E-4 s, completing the propagation from transmitter to receiver, as depicted in Figure 16.

The time-of-flight of the ultrasonic sound wave is determined by comparing the most prominent amplitude peak of the applied velocity, shown in Figure 8, to the received pressure signal, shown in Figure 17: Test case 1 COMSOL simulation: acoustic pressure pulse signal at receiver.. The peak of the applied velocity is at 3.80E-5 s, and the received pressure peak at the receiver is at 6.88E-4 s with an amplitude of 1.90E-9 Pa. From these measurements, the time-of-flight is calculated to be 6.50E-04 s.

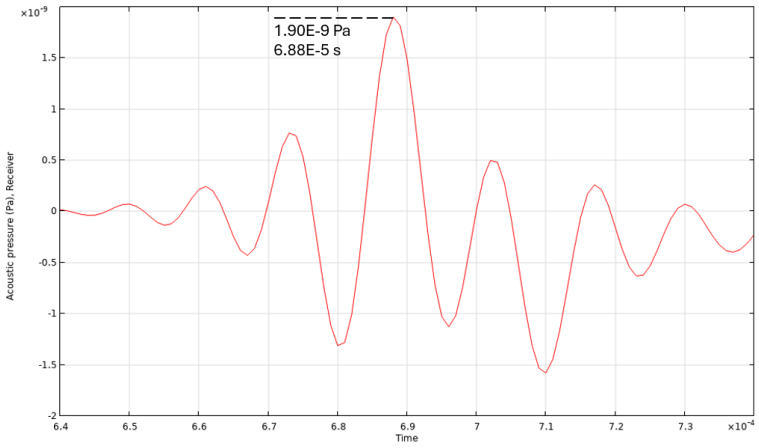

Figure 17: Test case 1 COMSOL simulation: acoustic pressure pulse signal at receiver.

7.1.3 Discussion

The simulation for Test case 1 accurately portrays the propagation path of the ultrasonic sound wave from transmitter to receiver by visualizing the dynamic pressure fluctuation. The time-of-flight of the ultrasonic sound wave was calculated to be 6.50E-4 s. This matches closely with [11], which reported identical time-of-flight. Additionally, the time-of-flight closely aligns with the analytical calculation of 6.54E-4 s from Chapter 5.1.1, yielding a difference of 0.70%. These findings demonstrate consistency across different models.

7.2 Test case 2: Normal - polycarbonate

7.2.1 Setup

Test case 2 modifies the setup of Test case 1, utilizing the same materials and temperature conditions. However, the geometry is changed where the transducers are angled normal to the plane of plate 1, as shown in Figure 10 and listed in

Table 2. The model comprises five domains, as described in Chapter 5. Domain 1 and 5, where the transducers are located, consist of ambient air at 20 °C. Domains 2 and 4 consist of polycarbonate. Domain 3 consists of the encapsulated air set to 20 °C.

The following series of figures (Figure 18 - Figure 21) depict the propagation of the ultrasonic sound wave through each domain to the receiver. Due to the orientation of the transducers, the ultrasonic sound wave travels in a straight line. Each figure displays five color scales, showcasing the total acoustic pressure in each domain. Thus, the color scales illustrating the wave propagation are domain-specific from 1 to 5.

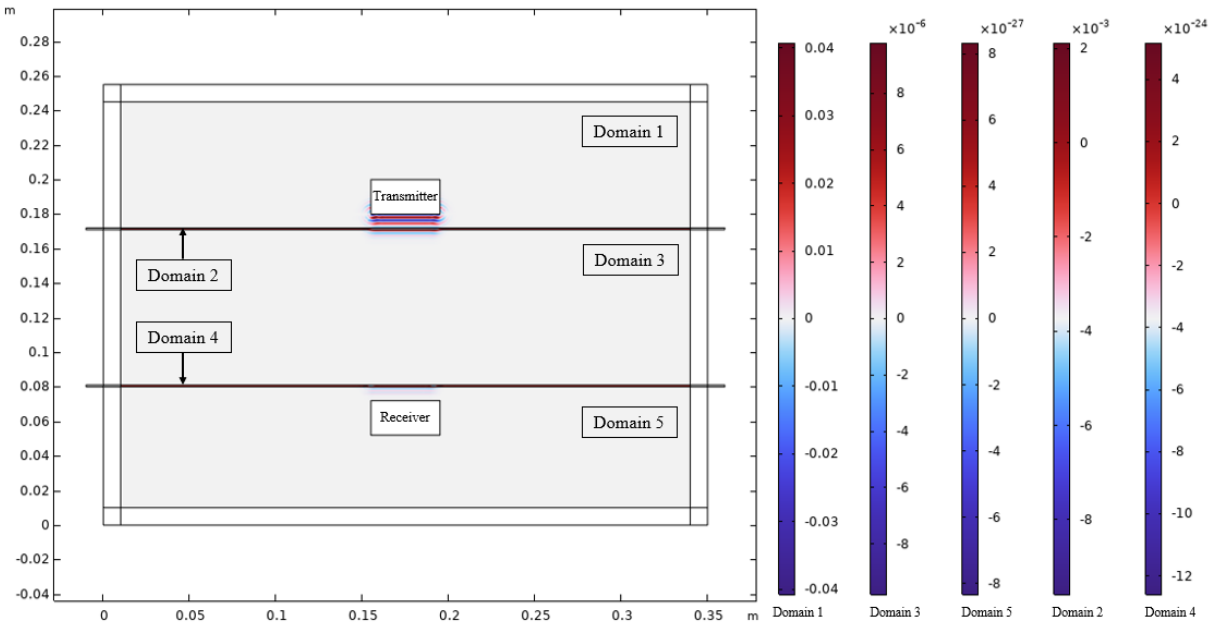

Figure 18: Test case 2 COMSOL simulation at 3.8E-5 s.

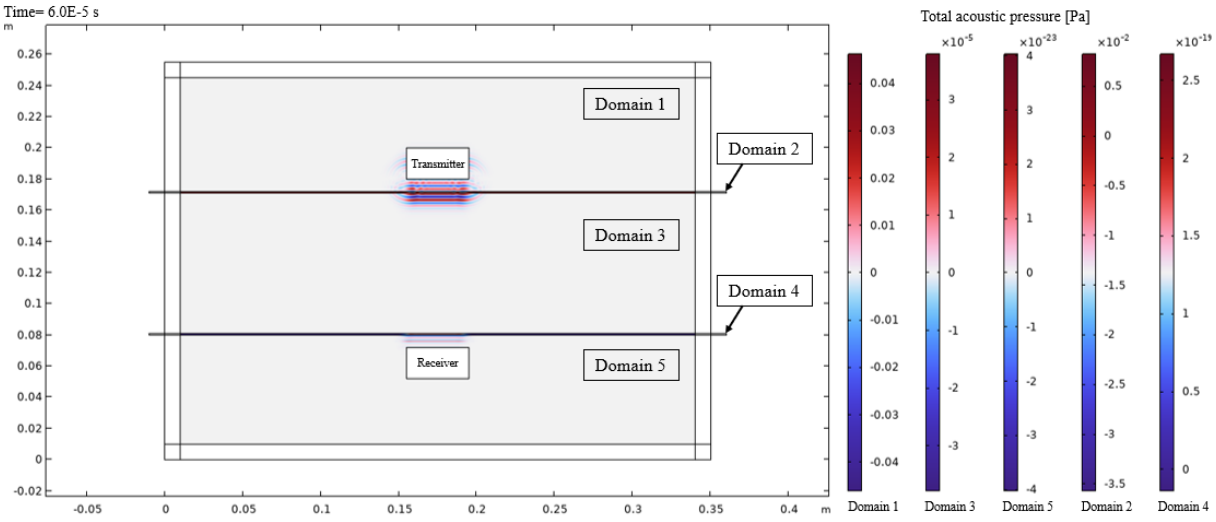

Figure 19: Test case 2 COMSOL simulation at 6.0E-5 s.

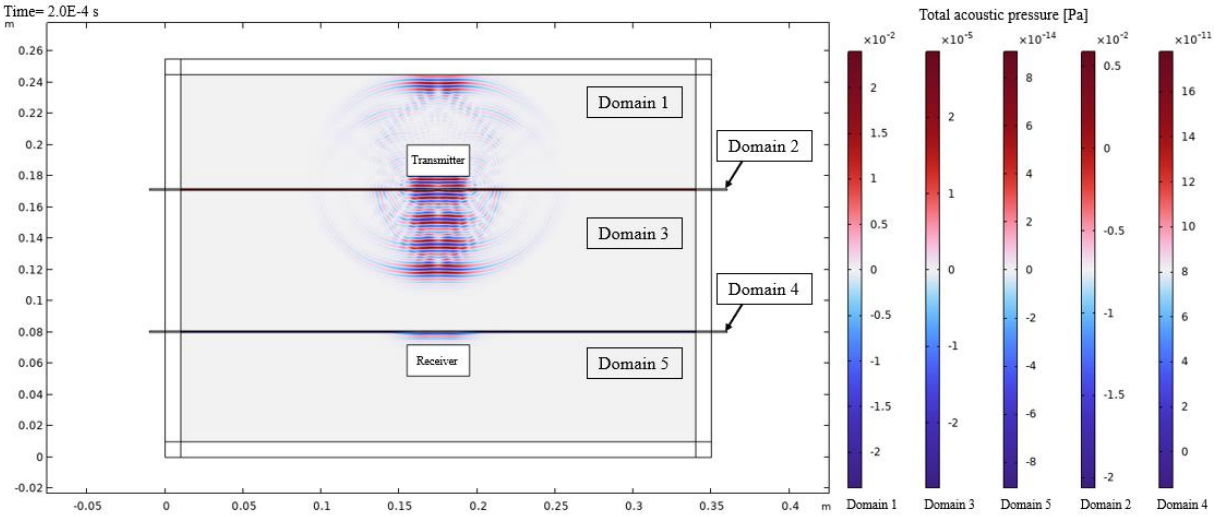

Figure 20: Test case 2 COMSOL simulation at 2.0E-4 s.

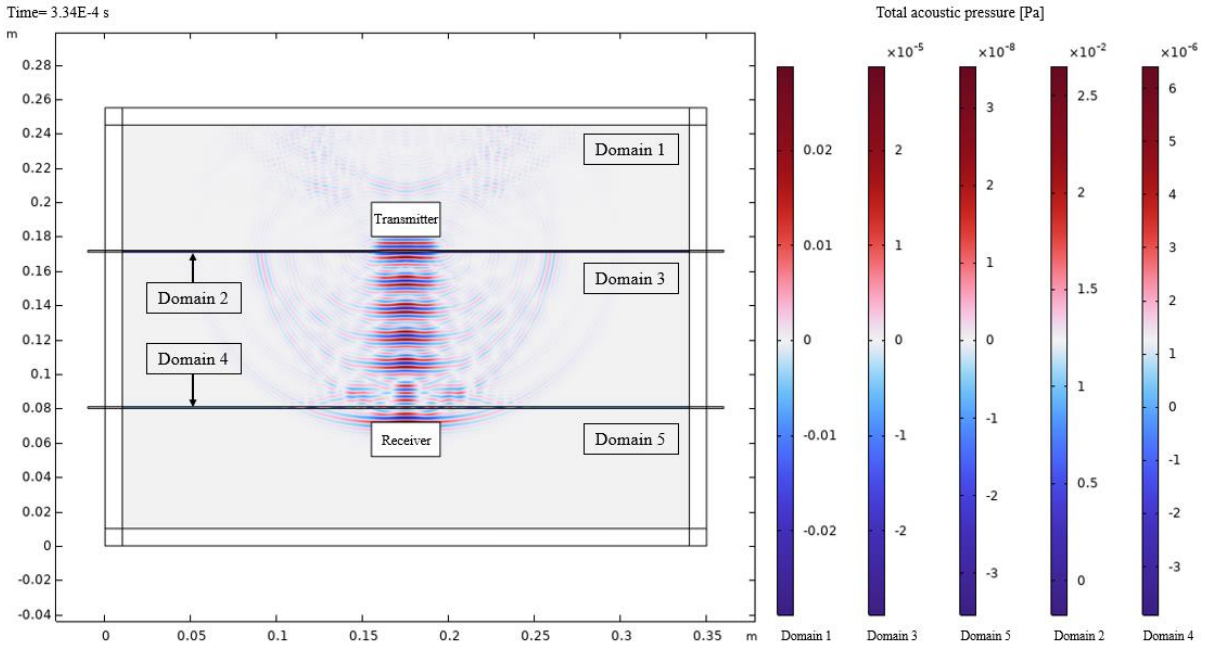

Figure 21: Test case 2 COMSOL simulation at 3.34E-4 s.

7.2.2 Simulation results and analysis

Figure 18 shows the initial ultrasonic sound wave emitted from the transmitter at 3.80E-5 s, propagating through domain 1 before reaching the polycarbonate plate in domain 2. Consistent with Test case 1, at the interface, the initial wave splits into two. Most of the energy is reflected back into Domain 1; the rest is transmitted into Domain 2. In Figure 19, the wave passes through the plate in domain 2 and continues the path into the encapsulated air in domain 3. The wave is then seen propagating through the encapsulated air in Figure 20. Consistent with Test case 1, the encapsulated air is set to 20 °C, corresponding to a speed of sound of 343.2 m/s, defined as a material property of the domain. Figure 21 captures the moment when the wave impacts the receiver at 3.34E-4 s, completing the propagation from transmitter to receiver.

As in test case 1, the time-of-flight of the ultrasonic sound wave is determined by comparing the most prominent peak of the applied velocity, shown in Figure 8, with the most prominent peak of the received pressure signal, shown in Figure 22. The peak of the applied velocity is at 3.80E-5 s, and the received pressure peak is at 3.34E-4 s with an amplitude of 2.55E-8 Pa. From these measurements, the time-of-flight is calculated to be 2.96E-4 s.

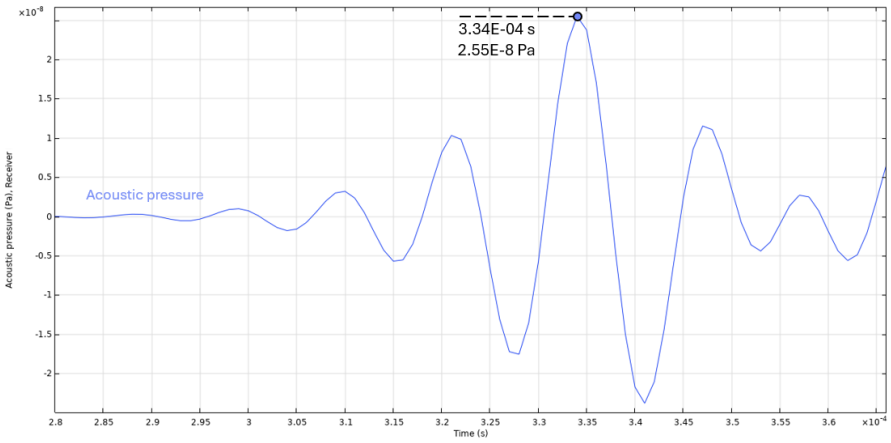

Figure 22: Test case 2 COMSOL simulation: Acoustic pressure signal at receiver.

7.2.3 Discussion

The simulation for Test case 2 visualize the vertical propagation path of the ultrasonic sound wave, in contrast with the oblique trajectory observed in Test case 1. The time-of-flight of the ultrasonic sound wave was calculated to be 2.96E-4 s, closely aligning with the analytical calculation of 3.10E-4 s from Chapter 5.1.2, yielding a difference of 4.67%. These finding demonstrates consistency across different models.

The time-of-flight in Test case 1 is slightly more aligned with the analytical calculations than in Test case 2. However, the received acoustic pressure signal in Test case 2 is considerably higher than Test case 1, demonstrating an improvement of the new geometrical model.

7.3 Test case 3: Normal – steel

7.3.1 Setup

Test case 3 expands on Test case 2 by modifying the material of the plates in domains 2 and 4 while retaining the same temperature conditions and geometry, as shown in Figure 10. In this test case, domains 2 and 4 are made of steel. The model comprises five domains, as described in Chapter 5. Domain 1 and 5 where the transducers are located consist of ambient air at 20 °C. Domain 2 and 4 consist of steel plates. Domain 3 consists of the encapsulated air set to 20 °C.

Consistent with the preceding cases, a series of figures (Figure 23-Figure 25) depicts the propagation of the ultrasonic sound pulse from the transmitter, through each domain, to the receiver. Despite the material change, the orientation of the transducers ensures a vertical propagation path. Each figure displays five color scales, showcasing the total acoustic pressure in each domain. Thus, the color scales illustrating the wave propagation are domain-specific from 1 to 5.

7.3.2 Hypothesized effect

The change to steel plates is expected to introduce significant difference in acoustic impedance mismatch, due to higher density and speed of sound compared to polycarbonate. This change in plate material is critical to the analysis, as they alter the wave propagation characteristics. It is expected that this change will reduce time-of-flight and increase reflected waves, thereby reducing the strength of the received signal.

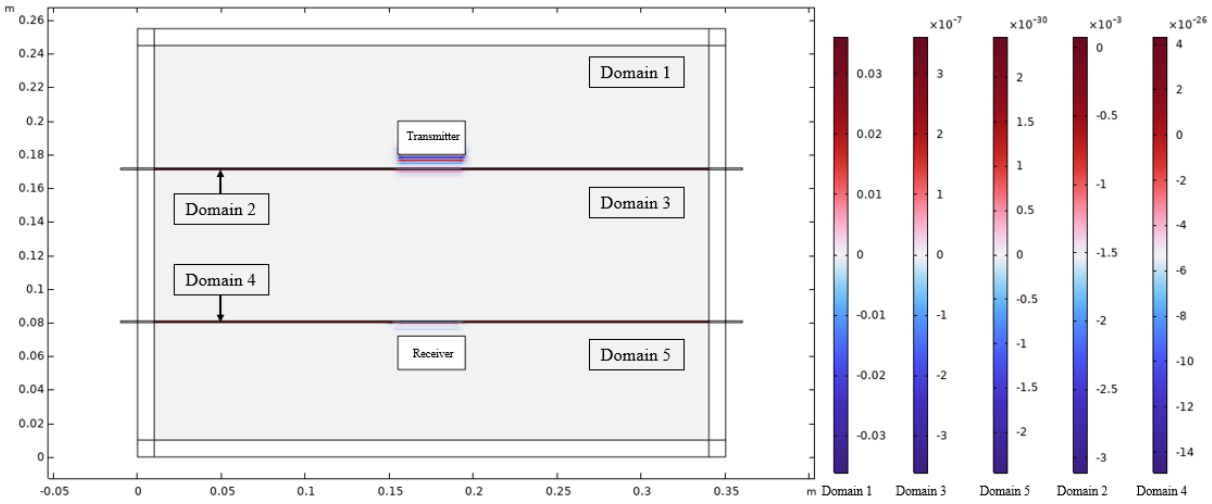

Figure 23: Test case 3 COMSOL simulation at 3.8E-5 s.

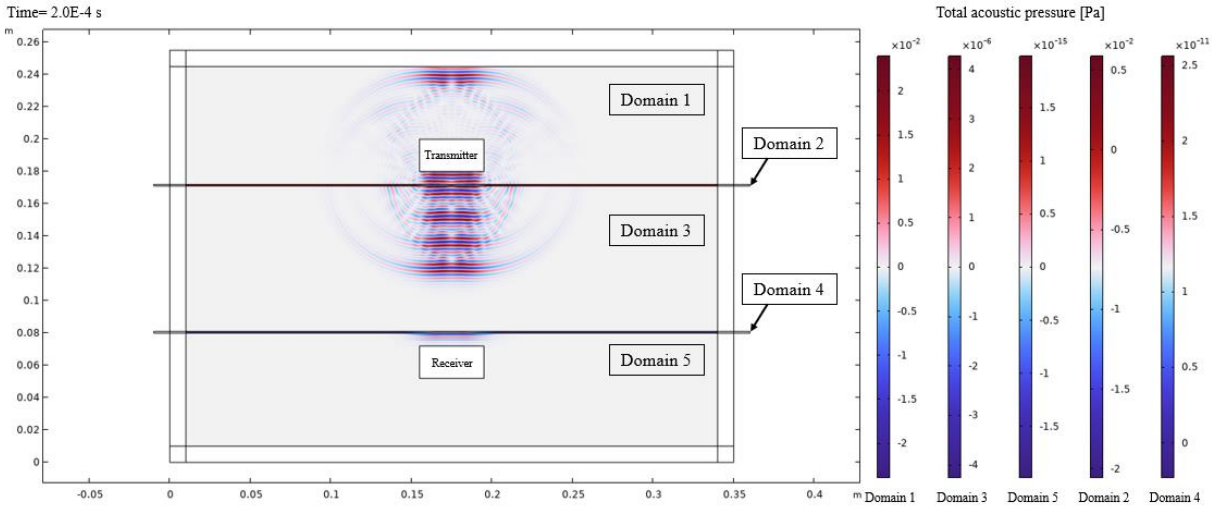

Figure 24: Test case 3 COMSOL simulation at 2.0E-4 s.

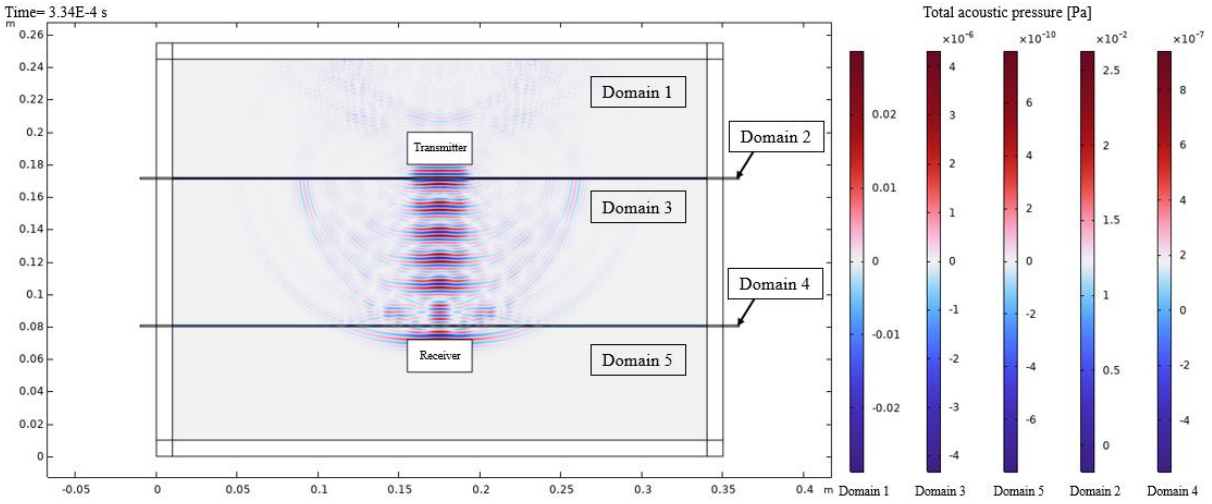

Figure 25: Test case 3 COMSOL simulation at 3.34E-4 s.

7.3.3 Simulation results and analysis

Figure 23 illustrates the initial ultrasonic sound wave emitted from the transmitter at 3.80 µs, propagating through domain 1, before reaching the steel in domain 2. As expected, an increased part of the wave is observed to be reflected at the interface with domain 2. This phenomenon is attributed to the acoustic impedance between the air in domain 1 and the steel in domain 2. In Figure 24, the wave passes through domain 2 and continues through the encapsulated air in domain 3. Consistent with Test case 2, the encapsulated air is set to 20 °C, corresponding to a speed of sound of 343.2 m/s, defined as a material property of the domain. Figure 25 captures the moment when the wave impacts the receiver at 3.34E-4 s, completing the propagation from transmitter to receiver.

As in previous cases, the time-of-flight of the ultrasonic sound wave is determined by comparing the most prominent peak of the applied velocity, shown in Figure 8, with the most prominent peak of the received pressure signal, shown in Figure 26. The peak of the applied velocity is at 3.80E-5 s, and the received pressure peak is at 3.34E-4 s with an amplitude of 5.75E-10 Pa. From this measurement, the time-of-flight is calculated to be 2.96E-4 s.

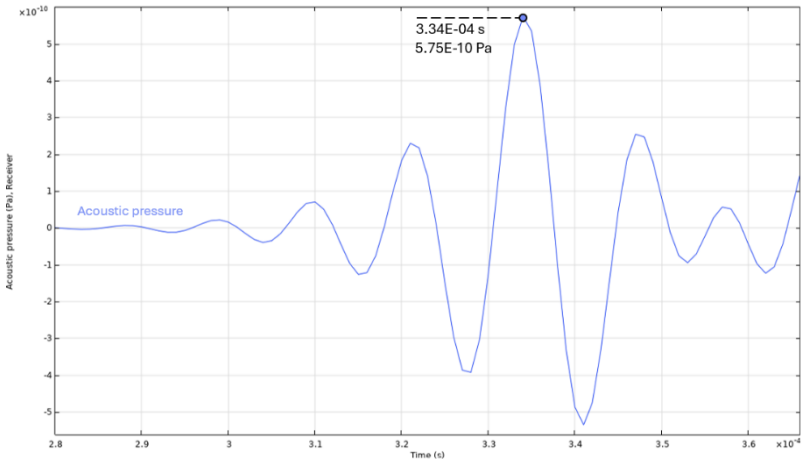

Figure 26: Test case 3 COMSOL simulation: Acoustic pressure signal at receiver.

7.3.4 Discussion

Test case 3 expands on Test case 2 by substituting the plate material with steel while maintaining other conditions constant. This modification explores the effect of a material with higher acoustic impedance on the propagating ultrasonic wave.

The simulation for Test case 3 captures the propagation of the ultrasonic sound wave from transmitter to receiver by visualizing the dynamic pressure fluctuation. Contrary to the anticipated result, the time-of-flight is measured to be 2.96E-4 s, identical to that of Test case 2. It was expected that the change to steel in domains 2 and 4 would reduce the time-of-flight since the speed of sound is greater in steel than in polycarbonate. However, the length of the plate domains is minimal compared to the total propagation length, arguably making the impact of the increased speed of sound negligible on the total time-of-flight. The time-of-flight closely aligns with the analytical calculation with a modest deviation of 4.31%, further confirming consistency across different models. Compared to Test case 2, the strength of the received acoustic pressure signal is weaker, with a received maximum pressure of 5.75E-10 Pa. These results highlight the significant impact of material properties on acoustic behavior, confirming the model's sensitivity to changes in acoustic impedance due to different materials. Comparing the outcomes with those in Test case 2, it is evident that the material changes lead to increased reflection and signal reduction. Although the time-of-flight remains constant due to the geometry, the material properties of steel amplify the loss in signal strength across the interfaces. This outcome underscores the challenges with acoustic thermometry in environments with high acoustic impedance mismatches, emphasizing the need for careful material selection in practical applications.

7.4 Test case 4: Normal – polycarbonate – high temperature

7.4.1 Setup

Test case 4 expands on Test case 2 by increasing the temperature of the encapsulated air in domain 3 while maintaining the same materials and geometry, as shown in Figure 10. In this model, the polycarbonate plates in domains 2 and 4 remain unchanged, but the temperature condition in domain 3 is set to 4000 °C. The domain configuration remains consistent with the setup described in Chapter 5. Domain 1 and 5, where the transducers are located, consist of ambient air at 20 °C. Domains 2 and 4 consist of polycarbonate plates. Domain 3 consists of the encapsulated air set to 4000 °C.

Consistent with the preceding test cases, a series of figures (Figure 27-Figure 29) depicts the propagation of the ultrasonic sound wave from the transmitter, through each domain, to the receiver. Each figure displays five color scales, showcasing the total acoustic pressure in each domain. Thus, the color scales illustrating the wave propagation are domain-specific from 1 to 5.

7.4.2 Hypothesized effect

The increase in temperature in domain 3 is expected to introduce a significant change in time-of-flight due to the effect of temperature on the speed of sound in the encapsulated air. In addition, it is hypothesized that the increase in temperature will cause a further reduction in signal strength at the receiver. As with the other test cases, it is expected that the acoustic pressure will vary notably between the domains due to the acoustic impedance mismatch. However, in Test case 4, it is expected an additional acoustic pressure drop at domain 3, due to the high temperature.

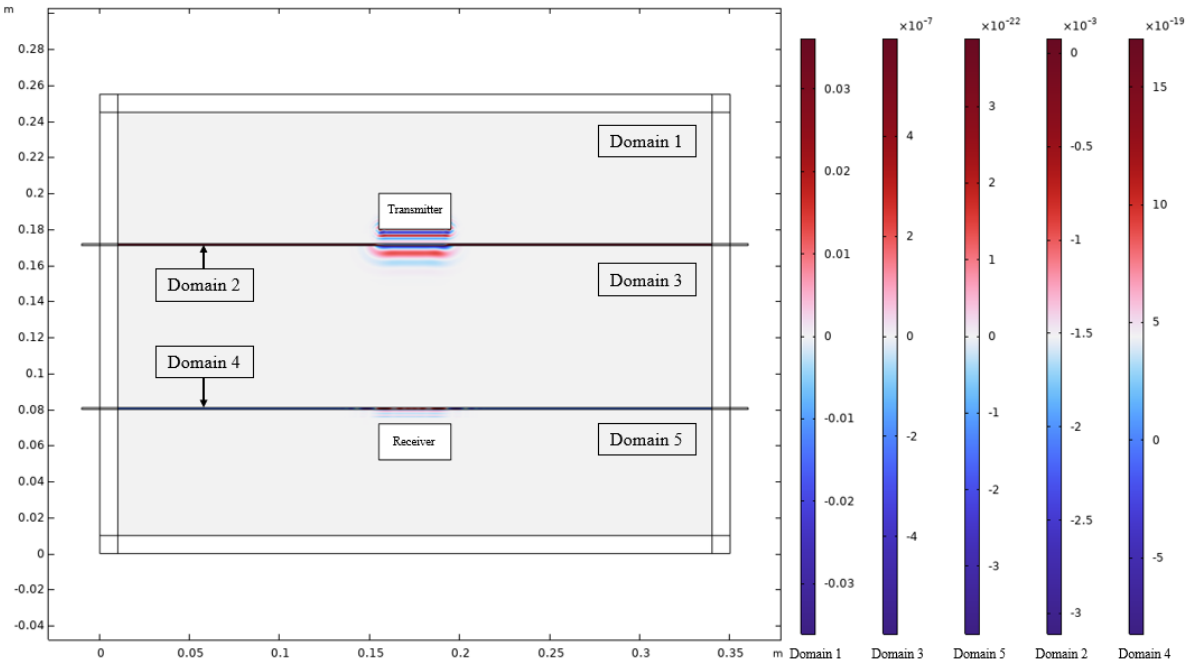

Figure 27: Test case 4 COMSOL simulation at 3.8E-5 s.

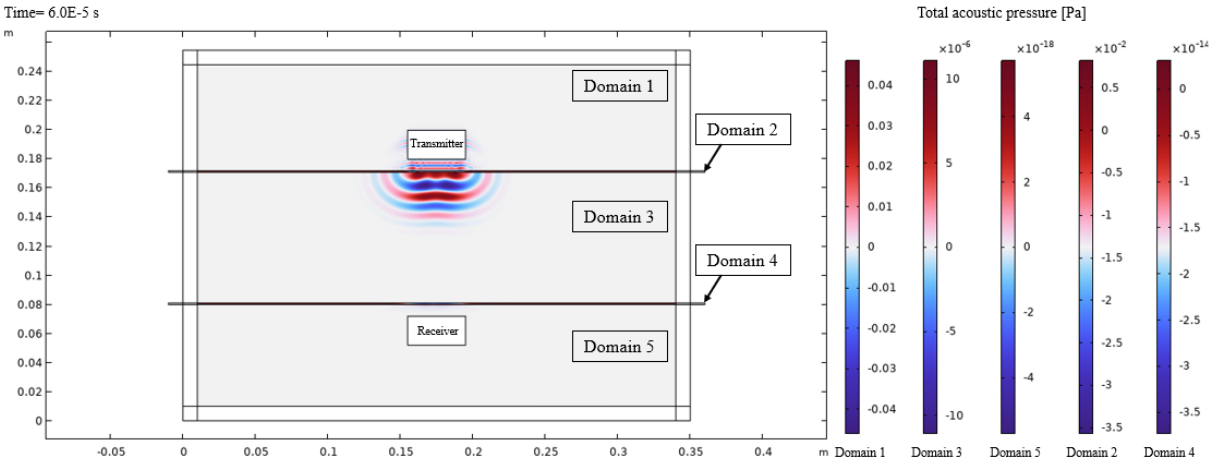

Figure 28: Test case 4 COMSOL simulation at 6.0E-5 s.

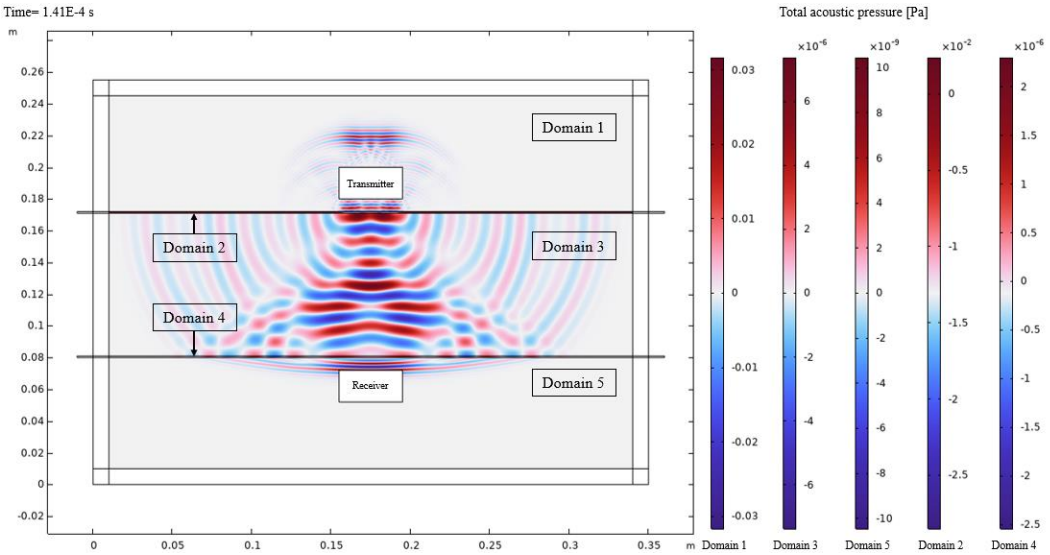

Figure 29:Test case 4 COMSOL simulation at 1.41E-4 s.

7.4.3 Simulation results and analysis

Figure 27 illustrates the initial ultrasonic sound wave emitted from the transmitter at 3.80E-5 s, propagating through domain 1 before reaching the polycarbonate plate in domain 2. Consistent with Test case 2, a significant part of the wave is observed to be reflected at the interface with domain 2. In Figure 28, the wave passes through domain 2 and continues into the encapsulated air in domain 3. In contrast to Test case 2, the encapsulated air is set to 4000 °C, corresponding to a speed of sound of 1310 m/s, defined as a material property for the domain. Figure 29 captures the moment when the wave impacts the receiver at 1.41E-4 s, completing the propagation from transmitter to receiver.

Consistent with the previous test cases, the time-of-flight is determined by comparing the most prominent peak of the applied velocity, shown in Figure 8, with the most prominent peak of the received pressure, shown in Figure 30. The peak of the applied velocity is at 3.38E-5 s, and the received pressure peak is 1.41E-4 s with an amplitude of 8.71E-9 Pa. From these measurements, the time-of-flight is calculated to be 1.03E-4 s.

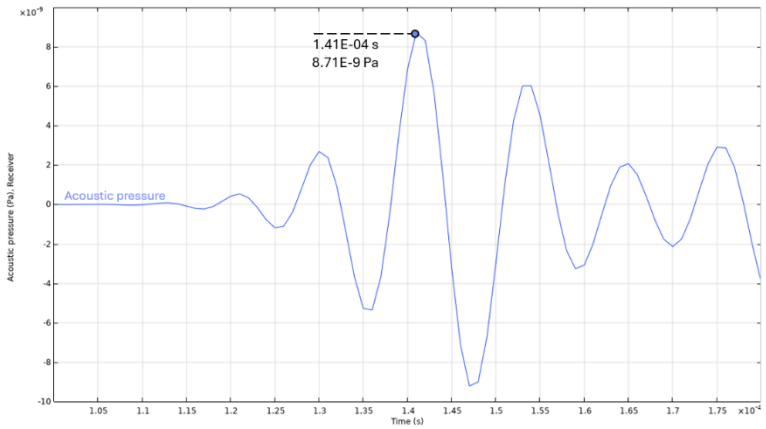

Figure 30:Test case 4 COMSOL simulation: Acoustic pressure signal at receiver.

7.4.4 Discussion

The simulation for Test case 4 captures the propagation of the ultrasonic sound wave from transmitter to receiver by visualizing the dynamic pressure fluctuation. As expected, the time-of-flight is substantially shorter than in Test case 2. This time difference is attributed to the increase in the speed of sound in the encapsulated air in domain 3 due to the increased temperature. The measured time-of-flight closely aligns the analytical calculations with a deviation of 6.75%, further confirming constancy across different models. Compared to Test case 2, the strength of the received acoustic pressure signal is weaker, with a received maximum pressure of 8.71E-9 Pa. This result highlights the impact of temperature changes on wave propagation. The temperature in domain 3 contributes to decreased signal strength, emphasizing the challenges with the method at elevated temperatures.

8 Discussion

The following sections will detail the results of the simulations and discuss their implications for practical applications.

Table 10 provides a summary of the times at which signals were detected at both the transmitter and receiver for each test case. These detection times are critical for evaluating the time-of-flight and the reduction in signal strength. The transmitter sends the wave across all the test cases at the same time. However, the detection times at the receiver vary across the test's cases, influenced by variations in geometry, materials, and temperature.

Test case 1 replicated the geometrical model used in [11] and served as a validation model for the computational approach in this study. The time-of-flight was equal to that in [11], supporting the validity of the computational model. In contrast to the other test cases, Test case 1 has its transducers oriented at an angle relative to the plane of the plates, resulting in a longer propagation path and, consequently, a longer time-of-flight.

In test cases 2-4, the geometry was modified with transducers oriented normally relative to the plane of the plates, resulting in a shorter propagation path. Test case 2, with the same material and temperature conditions as test case 1, as expected, was observed to have reduced time-of-flight, as seen in Table 10. Notably, a stronger pressure signal was detected at the receiver in test case 2 than in test case 1. Therefore, the new geometrical model developed in this study is arguably an improvement of the model in [11].

In test case 3, the plates are made of steel. Steel has a greater speed of sound than polycarbonate, as used in the previous test cases. Therefore, it was expected that the time-of-flight would decrease. However, the observed result indicates that this material change has a negligible effect on the time-of-flight. The thickness of the plate is small compared to the total propagation path, likely diminishing the impact of the increased speed of sound in this domain. However, as seen in Table 11, the received pressure signal is significantly decreased. This is likely due to the increased acoustic impedance mismatch at the plate interfaces, which causes increased reflections.

In test case 4, the temperature of the encapsulated air in domain 3 was increased to 4000 °C from the 20°C in the previous cases, with the corresponding speed of sound increasing from 343.2 m/s to 1310 m/s. As domain 3 is the longest section of the propagation path, the time-of-flight was expectedly the shortest of all simulations conducted, as seen in Table 10. Additionally, the increased temperature affected the received signal strength, resulting in a reduction compared to test case 2, as seen in Table 11.

Table 12 presents a comparison of the time-of-flight values between analytical calculations and simulation measurements for each test case, along with the percentage offset.

- Test Case 1: Displays the least offset at 0.70%, indicating high accuracy and model reliability under the tested conditions.
- Test Case 2 and 3: Display offsets of 4.67% and 4.31% respectively, which are still within acceptable limits, confirming the model's effectiveness across different scenarios.
- Test Case 4: Displays the highest offset at 11.88%, suggesting areas for model refinement, particularly under extreme conditions.

These results validate the computational model’s accuracy in simulating acoustic propagation and confirm its use for further practical applications. Each test case demonstrates that the model can reliably replicate expected physical phenomena, with discrepancies noted for further enhancement, especially under extreme conditions.

The primary objective of this model in a practical application such as a pressure vessel is to detect significant condition changes affecting the system, such as an arc fault in a switchgear. For its intended use within pressure vessels, the model functions as a temperature change detection system. The accuracy of predicting exact temperatures is less critical than the ability to detect deviations from expected time-of-flight values.

The functionality of the system is as follows: a transmitter sends a signal expected to be detected by the receiver within a predetermined time frame based on the standard operating temperatures. A signal not detected within this time frame indicates an anomaly likely caused by a temperature change. This anomaly would automatically trigger an alarm, prompting a response to address potential safety or operational concerns.

The crucial factor is the reliability in detecting and triggering an alarm when the received signal falls outside the expected time-of-flight range, thereby providing a safety mechanism for pressure vessels.

Table 10: Detected signal times and time-of-flight in simulations.

Time of wave detection			
Test case:	Transmitter [s]:	Receiver [s]:	Time-of-flight [s]:
Test case 1	3.80E-05	6.880E-04	6.50E-04
Test case 2	3.80E-05	3.340E-04	2.96E-04
Test case 3	3.80E-05	3.340E-04	2.96E-04
Test case 4	3.80E-05	1.410E-04	1.03E-04

Table 11: Acoustic pressure detected in simulations.

Acoustic pressure	
Test case:	Receiver [Pa]:
Test case 1	1.903E-09
Test case 2	2.553E-08
Test case 3	5.747E-10
Test case 4	8.716E-09

Table 12: Time-of-flight comparison between analytical calculations and simulated values.

Time-of-flight comparison			
Test case:	Calculated value [s]:	Simulated value [s]:	Offset [%]:
Test case 1	6.55E-04	6.50E-04	0.70
Test case 2	3.10E-04	2.96E-04	4.67
Test case 3	3.09E-04	2.96E-04	4.31
Test case 4	1.17E-04	1.03E-04	11.88

9 Conclusion

9.1 Conclusion

The objective of this study is to address the challenges of detecting a temperature increase inside a pressure vessel through a non-invasive method, ensuring that preventive actions can be taken before equipment failure occurs. This study proposes the use of transducers transmitting ultrasonic sound waves through the pressure vessel. This method leverages the principle that the speed of sound varies with temperature. The proposed solution was tested by developing a computational model, building on the work done in [11]. This model was further validated by comparing its output with analytical calculations.

This study has demonstrated state change inside a pressure vessel using a non-invasive ultrasonic method through simulations. The key findings show that the computational model is capable of measuring the time-of-flight of ultrasonic waves, which varies with temperature fluctuations inside the vessel. Each test case provided important insights into how different conditions affected the model output:

- Test case 1 confirmed the model's validity by comparison to previous work done in [11].
- Test case 2 demonstrated improvements in the geometric model. It reduced the time-of-flight and showed stronger pressure signals at the receiver, suggesting better detection capabilities than those in Test case 1.
- Test case 3 revealed that material changes to steel did not significantly affect the time-of-flight due to the small thickness of the plates.
- Test case 4 highlighted the model's sensitivity to extreme temperatures. The increased temperature substantially shortened the time-of-flight and weakened signal strength.

This research highlights the potential of using ultrasonic methods as a non-invasive alarm system for preventive measures in industrial applications. The ability to detect temperature changes within pressure vessel non-invasively, provides a significant advantage in operational safety and efficiency.

9.2 Further work

The natural progression of this study leads to the next step: conducting physical experiments. These experiments are vital for validating the theoretical model under real-world conditions. The plan to include physical testing was established early in the research. However, due to time constraints, it was not possible to include this phase in this study. The following work is advised for a physical experiment:

1. Selection of transducers: Transducer capable transmitting sound waves with frequency of 100 kHz and detect pressure signals of at least 5.7E-10 Pa, must be selected.
2. Constructions of mock containment system: A containment system must be designed to mimic the simulated environment. The initial experiment will use materials with low acoustic impedance to minimize signal distortion and maximize measurement accuracy. This approach will minimize signal interference and establish a baseline for measuring the interaction between ultrasonic waves and containment materials.
3. Gradual experimentation: Aligning with the approach in the simulations, the physical experiment will be developed gradually. Starting with conditions from test case 2, the experiments will progressively introduce variables like different materials and temperatures. This approach allows for precise adjustments and analysis of the impact of each variable.

These experiments aim to verify the computational model under real-world conditions. They will confirm the ultrasonic method's ability to detect temperature changes in the mock containment and evaluate its limitations under various conditions.

References

[1] B. Hayes, "Six case histories of pressure vessel failures," *Engineering Failure Analysis,* vol. 3, no. 3, pp. 157-170, 1996.

[2] Y. A. Cengel, M. A. Boles, and M. Kanoğlu, *Thermodynamics: an engineering approach*. McGraw-hill New York, 2011.

[3] T. Claggett, R. Worrall, and B. Liptak, "Thermocouples," in *Temperature Measurement*: CRC Press, 2022, pp. 95-118.

[4] B. D. MacDonald and A. M. Rowe, "Experimental and numerical analysis of dynamic metal hydride hydrogen storage systems," *Journal of Power Sources,* vol. 174, no. 1, pp. 282-293, 2007.

[5] N. F. o. S. a. Technology. "Kunstig intelligens ved REALTEK." https://www.nmbu.no/fakulteter/fakultet-realfag-og-teknologi/kunstig-intelligens-ved-realtek (accessed 13. Mai, 2024).

[6] M. A. Langerman, G. Larsen, and R. Pendleton, "The Effect of Elevated Temperatures on the Failure of Unfired Pressure Vessels," in *ASME International Mechanical Engineering Congress and Exposition*, 2003, vol. 37092, pp. 1-6.

[7] J. Douchin and F. Gentils, "Pressure rise in switchgear rooms in case of internal arc in AIS MV switchboards: Importance of room design and simplified calculation method," 2013.

[8] S. Singh, D. S. Thevar, and O. Granhaug, "Internal arc root movement and burnthrough prediction by simulation using first principle," in *CIRED 2021-The 26th International Conference and Exhibition on Electricity Distribution*, 2021, vol. 2021: IET, pp. 35-40.

[9] B. R. Tittmann, "Sonic pressure vessel sensor," 2005.

[10] N. J. Miller and S. W. Shaw, "Frequency sweeping with concurrent parametric amplification," 2012.

[11] Z. Fan, W. Jiang, and W. M. D. Wright, "Non-contact ultrasonic gas flow metering using air-coupled leaky Lamb waves," *Ultrasonics,* vol. 89, pp. 74-83, 2018/09/01/ 2018, doi: https://doi.org/10.1016/j.ultras.2018.04.008.

[12] A. Bedford and D. S. Drumheller, *Introduction to elastic wave propagation*. Springer Nature, 2023.

[13] Iowa State University Center for Nondestructive Evaluation (CNDE). "Physics of Nondestructive Evaluation." https://www.nde-ed.org/Physics/Sound/index.xhtml (accessed 14. Feb, 2024).

[14] D. Russell. "Longitudinal and Transverse Wave Motion." The Pennsylvania State University. https://www.acs.psu.edu/drussell/Demos/waves/wavemotion.html (accessed 14. Feb, 2024).

[15] W. Moebs, S. J. Ling, and J. Sanny, *University Physics Volume 1*: OpenStax, 2016. [Online]. Available:

https://openstax.org/books/university-physics-volume-1/pages/1-introduction.
[16] L.E. Kinsler, A.R. Frey, A.B. Coppens, J.V. Sanders, *Fundamentals of Acoustics*, 4th ed. John Wiley & Sons, 2000.
[17] J. Wortman and R. Evans, "Young's modulus, shear modulus, and Poisson's ratio in silicon and germanium," *Journal of applied physics,* vol. 36, no. 1, pp. 153-156, 1965.
[18] R. E. Apfel, "Technique for measuring the adiabatic compressibility, density, and sound speed of submicroliter liquid samples," *The Journal of the Acoustical Society of America,* vol. 59, no. 2, pp. 339-343, 1976.
[19] J. Walker, D. Halliday, R. Resnick, *Fundamentals of physics*, 10 ed. John Wiley & Sons, Inc, 2014.
[20] J.-P. Dalmont, "Acoustic impedance measurement, Part I: A review," *Journal of Sound and Vibration,* vol. 243, no. 3, pp. 427-439, 2001.
[21] "What is Switchgear?" ASCO Power Technologies. https://www.ascopower.com/us/en/resources/articles/what-is-switchgear.jsp (accessed 29. Jan, 2024).
[22] J. Parry, "Mechanical aspects in the design of distribution switchgear," *Electronics & Power,* vol. 25, no. 2, pp. 127-130, 1979.
[23] M. Binnendiljk, G. Schoonenberg, and A. Lammers, "The prevention and control of internal arcs in medium-voltage switchgear," 1997.
[24] SiemensAG, "Arc Faults in Medium-Voltage Switchgear and Low-Voltage Switchboards." [Online]. Available: https://assets.new.siemens.com/siemens/assets/api/uuid:c4054fd96445e7c54b3c0b390814e6cffc72ee2f/07-arcing-faults-in-medium-and-low-voltage-switchgear.pdf
[25] M. Desborough, "Pressure rise and burn through predictions and the principles of pressure relief device design [of gas-insulated switchgear]," in *IEE Colloquium on Risk Reduction: Internal Faults in T&D Switchgear (Digest No: 1997/295)*, 1997: IET, pp. 1/1-1/6.
[26] D. Rochette, S. Clain, W. Bussiere, P. André, and C. Besnard, "Porous filter optimization to improve the safety of the medium-voltage electrical installations during an internal arc fault," *IEEE transactions on power delivery,* vol. 25, no. 4, pp. 2464-2471, 2010.
[27] G. Hussain, M. Shafiq, and M. Lehtonen, "Predicting arc faults in distribution switchgears," in *2016 17th International Scientific Conference on Electric Power Engineering (EPE)*, 2016: IEEE, pp. 1-6.
[28] Y. Wu *et al.*, "Experimental and theoretical study of internal fault arc in a closed container," *Journal of Physics D: Applied Physics,* vol. 47, no. 50, p. 505204, 2014.

[29] Z. Li, J. Wang, X. Zhou, S. Huang, R. Yan, and Z. Xia, "Influence of chamber structure on arc quenching in multigap system," *High Voltage,* vol. 5, no. 3, pp. 313-318, 2020.
[30] COMSOL AB. "Acoustics Module User's Guide." COMSOl AB. https://doc.comsol.com/5.4/doc/com.comsol.help.aco/AcousticsModuleUsersGuide.pdf (accessed 2024).
[31] A. Klöckner, T. Warburton, and J. S. Hesthaven, "Viscous shock capturing in a time-explicit discontinuous Galerkin method," *Mathematical Modelling of Natural Phenomena,* vol. 6, no. 3, pp. 57-83, 2011.
[32] I. S. Raju, "The discontinuous galerkin finite element method," 2022.

Norges miljø- og biovitenskapelige universitet
Noregs miljø- og biovitskapelege universitet
Norwegian University of Life Sciences

Postboks 5003
NO-1432 Ås
Norway